เส้นใยอิเล็กโทรสปันซิลเวอร์/อะลูมินาสำหรับการกำจัดสีย้อมเมทิลีนบลู

นายปรม ไวกสิการ

วิทยานิพนธ์นี้เป็นส่วนหนึ่งของการศึกษาตามหลักสูตรปริญญาวิทยาศาสตรมหาบัณฑิต
สาขาวิชาปิโตรเคมีและวิทยาศาสตร์พอลิเมอร์
คณะวิทยาศาสตร์ จุฬาลงกรณ์มหาวิทยาลัย
ปีการศึกษา 2559
ลิขสิทธิ์ของจุฬาลงกรณ์มหาวิทยาลัย

ELECTROSPUN Ag/Al$_2$O$_3$ FIBERS FOR REMOVAL OF METHYLENE BLUE

Mr. Parom Waikasikarn
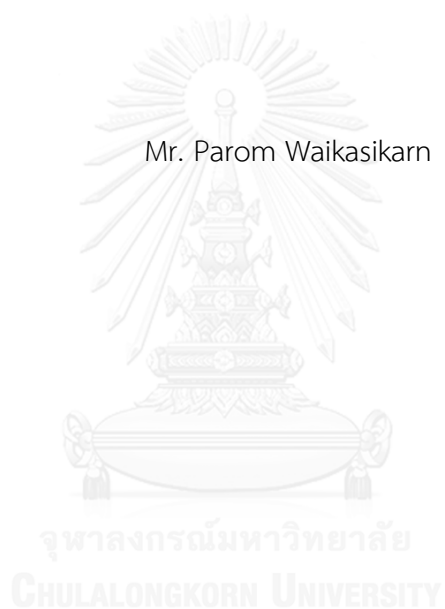
A Thesis Submitted in Partial Fulfillment of the Requirements

for the Degree of Master of Science Program in Petrochemistry and Polymer Science

Faculty of Science

Chulalongkorn University

Academic Year 2016

Thesis Title	ELECTROSPUN Ag/Al$_2$O$_3$ FIBERS FOR REMOVAL OF METHYLENE BLUE
By	Mr. Parom Waikasikarn
Field of Study	Petrochemistry and Polymer Science
Thesis Advisor	Assistant Professor Puttaruksa Varanusupakul, Ph.D.

Accepted by the Faculty of Science, Chulalongkorn University in Partial Fulfillment of the Requirements for the Master's Degree

....Dean of the Faculty of Science

(Associate Professor Polkit Sangvanich, Ph.D.)

THESIS COMMITTEE

....Chairman

(Professor Pattarapan Prasassarakich, Ph.D.)

....Thesis Advisor

(Assistant Professor Puttaruksa Varanusupakul, Ph.D.)

....Examiner

(Associate Professor Kawee Srikulkit, Ph.D.)

....External Examiner

(Assistant Professor Jinda Yeyongchaiwat, Ph.D.)

ปรม ไวกสิการ : เส้นใยอิเล็กโทรสปันซิลเวอร์/อะลูมินาสำหรับการกำจัดสีย้อมเมทิลีนบลู (ELECTROSPUN Ag/Al₂O₃ FIBERS FOR REMOVAL OF METHYLENE BLUE) อ.ที่ปรึกษาวิทยานิพนธ์หลัก: ผศ. ดร.พุทธรักษา วรานุศุภากุล, 63 หน้า.

ในงานวิจัยนี้ได้เตรียมเส้นใยอิเล็กโทรสปันซิลเวอร์/อะลูมินาโดยเตรียมจากเทคนิคโซลเจลอิเล็กโทรสปินิงเพื่อใช้ในการกำจัดสีย้อมเมทิลีนบลูโดยผ่านการดูดซับร่วมกับการย่อยสลายโดยใช้แสง ในงานวิจัยนี้เส้นใยอิเล็กโทรสปันซิลเวอร์/อะลูมินาถูกเตรียมโดยใช้ปริมาณซิลเวอร์ที่แตกต่างกัน (2,5 และ 10% โดยน้ำหนัก) และนำไปแคลไซน์ที่อุณหภูมิแตกต่างกัน (350 และ 500 องศาเซลเซียส) เส้นใยอิเล็กโทรสปันซิลเวอร์/อะลูมินาถูกตรวจสอบลักษณะเฉพาะด้วยเทคนิค SEM, TEM, FTIR, UV-VIS, XRD และการดูดซับและคายซับแก๊สไนโตรเจน จากการตรวจสอบพบว่าอะลูมินาที่ได้อยู่ในรูปของแกมมาและมีขนาดเส้นผ่านศูนย์กลางเฉลี่ยของเส้นใยมีขนาดประมาณ 75 นาโนเมตร เส้นผ่านศูนย์กลางเฉลี่ยของอนุภาคซิลเวอร์อยู่ในช่วง 3 ถึง 13 นาโนเมตร นอกจากนั้นยังพบว่าซิลเวอร์ที่อยู่บนอะลูมินาอยู่ในรูปของอนุภาคซิลเวอร์และซิลเวอร์ออกไซด์ จากนั้นนำเส้นใยอิเล็กโทรสปันซิลเวอร์/อะลูมินาไปทำการกำจัดสีย้อมเมทิลีนบลูพบว่า เส้นใยอะลูมินามีความสามารถในการดูดซับสีย้อม 54.8% อย่างไรก็ตามเมื่อนำตัวอย่างเส้นใย 10% โดยน้ำหนักของซิลเวอร์/อะลูมินาที่ทำการแคลไซน์ที่อุณหภูมิ 350 องศาเซลเซียสไปทำการย่อยสลายสีย้อมโดยใช้แสงพบว่ามีความสามารถในการกำจัดสีย้อมมากกว่าเส้นใยอะลูมินาถึง 2 เท่า (เส้นใยอะลูมินาสามารถกำจัดสีย้อมได้ 25% และเส้นใย 10% โดยน้ำหนักของซิลเวอร์/อะลูมินาที่ทำการแคลไซน์ที่อุณหภูมิ 350 องศาเซลเซียส สามารถกำจัดสีย้อมได้ 48%) จากผลการทำลองสรุปได้ว่า เส้นใย 10% โดยน้ำหนักของซิลเวอร์/อะลูมินาที่ทำการแคลไซน์ที่อุณหภูมิ 350 องศาเซลเซียส มีความสามารถในการกำจัดสีย้อมได้สูงที่สุดที่ 95.3% (สามารถทำการดูดซับได้ 47.3% และย่อยสลายโดยใช้แสงได้ 48%) นอกจากนั้นตัวอย่างเส้นใยอิเล็กโทรสปันซิลเวอร์/อะลูมินายังสามารถเก็บและนำมาใช้ซ้ำได้ถึง 3 ครั้งโดยไม่สูญเสียประสิทธิภาพในการกำจัดสีย้อมโดยใช้แสง

5772283123 : MAJOR PETROCHEMISTRY AND POLYMER SCIENCE

KEYWORDS:

PAROM WAIKASIKARN: ELECTROSPUN Ag/Al_2O_3 FIBERS FOR REMOVAL OF METHYLENE BLUE. ADVISOR: ASST. PROF. PUTTARUKSA VARANUSUPAKUL, Ph.D., 63 pp.

In this work, electrospun Ag/Al_2O_3 fibers were prepared by the sol–gel electrospinning methods in order to apply as sorbent and catalyst in photocatalytic reaction for removal of methylene blue. The electrospun Ag/Al_2O_3 fibers at various silver concentrations (2, 5 and 10%w/w) and different calcination temperatures (350 and 500 $^{\circ}$C) were prepared. The electrospun Ag/Al_2O_3 fibers were characterized by scanning electron microscopy (SEM), transmission electron microscopy (TEM), Fourier transform infrared spectroscopy (FTIR), UV-VIS spectroscopy, X-ray Diffraction Analysis (XRD) and nitrogen adsorption/desorption analysis. The phase of alumina in Ag/Al_2O_3 fibers was gamma-alumina phase and the average diameter of obtained fibers was 75 nm. The average diameters of silver particles in Ag/Al_2O_3 fibers ranged from 3 to 13 nm and were in the form of Ag^0 and Ag_2O. Then the electrospun Ag/Al_2O_3 fibers were applied for the removal of methylene blue in water. The removal efficiency of methylene blue by adsorption process was mainly from the host alumina which showed the percent removal of 54.8%. However, the calcined 10%w/w Ag/Al_2O_3 fibers at 350°C enhanced the removal efficiency of methylene blue by photocatalytic degradation approximately 2 times (% removal of methylene blue was 25% for Al_2O_3 and 48% for calcined 10%w/w Ag/Al_2O_3 fibers at 350°C). As a result, the Ag/Al_2O_3 fibers (calcined 10%w/w Ag/Al_2O_3 fibers at 350°C) exhibited the great effectiveness in the removal of methylene blue in water with 95.3% removal (47.3% by adsorption process and 48.0% by photocatalytic degradation). In addition, the electrospun Ag/Al_2O_3 fibers were easily collected and can be reused up to 3 times without the loss of photocatalytic degradation performance.

Field of Study: Petrochemistry and   Student's Signature ....
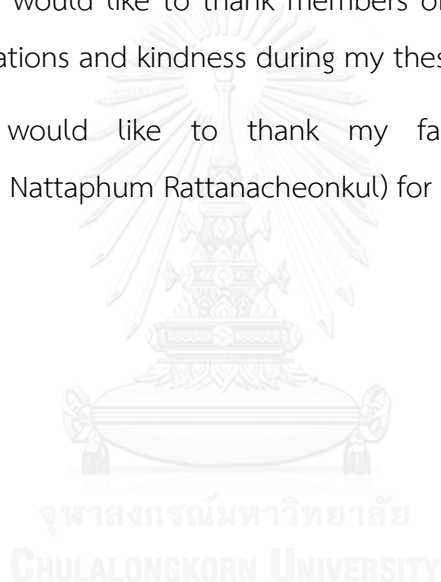
Polymer Science   Advisor's Signature ....

Academic Year: 2016

ACKNOWLEDGEMENTS

CONTENTS

LIST OF TABLES

LIST OF FIGURES

CHAPTER I
INTRODUCTION

1.1 Statement of purpose

Dyes are emitted into wastewater from various industries such as dye manufacturing and textile dyeing. It affects many problems when they discharged to environment. The water coloration from the presence of dyes, even in small amount of dyes, is highly visible. It causes a decrease in light penetration and gas solubility of water which might affect ecological balance. The treatment techniques for removal of dyes from wastewater, are adsorption and photocatalytic degradation, which is one of the effective techniques to remove dyes from wastewater. Adsorption process using alumina as adsorbent has been applied in wastewater treatment due to many advantages, such as large surface area, good thermal stability, cheap and simple material.

In recent years, ceramic with nanostructures has been researched. Preparation of various metal oxide fibers by the electrospinning technique in conjunction with the sol-gel technique are studied and reported. The electrospun fibers of metal oxides have many benefits for example micrometer down to nanometer range of fiber diameters, high surface area to volume ratio, low resistance to flow of liquid through the fibers and the simple technique.

Fumio Suzuki [1] studied the formation and mechanical properties of polyvinyl alcohol/alumina gel composite. An alumina sol was prepared from aluminium iso-propoxide (AIP). The alkoxide was hydrolyzed and peptized to a clear sol with acetic acid as a catalyst. The results showed that alumina mixed homogenously with PVA.

Jeon-Hee Kim [2] prepared alumina nanofibers which combining the sol–gel and electrospinning methods using AIP as an alumina precursor. A series of phase transitions of alumina when varied a calcination temperature from 500℃ to 1,200℃ were observed. The phase of alumina were changing from boehmite to γ-alumina and then to α-alumina. γ-alumina showed the highest surface area resulting to the highest removal efficiency of dye pollutant.

In addition, photocatalytic degradation of dyes in wastewater using semiconductive particles, such as titanium dioxide, has been reported. Semiconductive particle is very useful in removing dyes by photocatalytic activity under the presence of UV light. For practical applications, metal nanoparticles and some semiconductive particles such as silver oxide were also reported as an effective photocatalyst for dyes removal under visible light illumination. However, controlled synthesis of silver nanoparticles in the aqueous solution was difficult in producing long-term stable particles and cannot be reused [3-5].

Saranya Vadakara [6] studied the synthesis of silver nanoparticles (AgNPs) using Casuarina equisetifolia leaf extract. The photocatalytic activity of the synthesized silver nanoparticles was observed to have potential efficacy to degrade methylene blue dye under sunlight irradiation. The synthesized silver nanoparticles effectively degraded nearly 35.13% of methylene blue dye at 5 hours of exposure time.

In 2012, Kuang-Hsiu Chen [7] prepared Ag-decorated SiO_2 nanosphere for removal of dye by photodegradation. The photocatalyst performance of Ag-decorated SiO_2 nanosphere was evaluated under natural sunlight. As a result, the Ag-decorated SiO_2 nanosphere can be used and gave highly efficiency of photocatalyst.

Wei Jiang [8] prepared silver oxide nanoparticle for decomposition of organic pollutants. The results showed that methyl orange (MO) was decomposed completely in 120 seconds under irradiation of sunlight. Moreover, the photocatalytic

performance of as-prepared silver oxide remained almost constant after reuse or exposure under sunlight.

Therefore, in this work, the alumina fibers were synthesized via electrospinning in conjunction of sol-gel techniques. Silver was incorporated by conventional impregnation to produce Ag/Al_2O_3. Then, the removal of methylene blue dyes, which have shown in Figure 1.1, by the synthesized sorbent will thoroughly be investigated. Both adsorption and photocatalytic degradation of methylene blue dye were studied to improve efficiency of removal of methylene blue dye. Moreover, reusability of the sorbent was also examined.
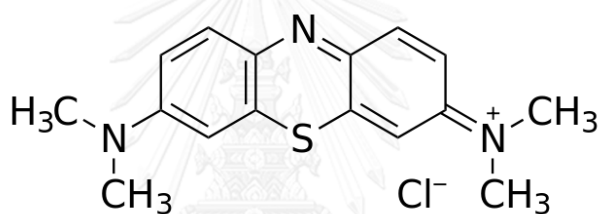
Figure 1.1 Methylene blue dye.

1.2 Objective

1. To synthesize the Ag/Al_2O_3 fibers via electrospinning in conjunction of sol-gel techniques.

2. To investigate the efficiency of the adsorption and photocatalytic degradation   of methylene blue dye.

1.3 Scope of research works

The scope of this research is limited in laboratory scale as follows:

1. Preparation of Al_2O_3 fibers by electrospinning sol-gel techniques using polyvinyl alcohol as a template agent in the electrospinning techniques and aluminium isopropoxide as a precursor in the sol-gel techniques.

2. Impregnation the Ag on Al_2O_3 by conventional impregnation and calcination at 350 and 500 $^{\circ}$C.

3. Removal of the methylene blue dye from water by synthesized Ag/Al_2O_3 via adsorption and photocatalytic degradation.

1.4 Expected benefits

The Ag/Al_2O_3 fibers were prepared and used as a sorbent for the removal of methylene blue dye from water.
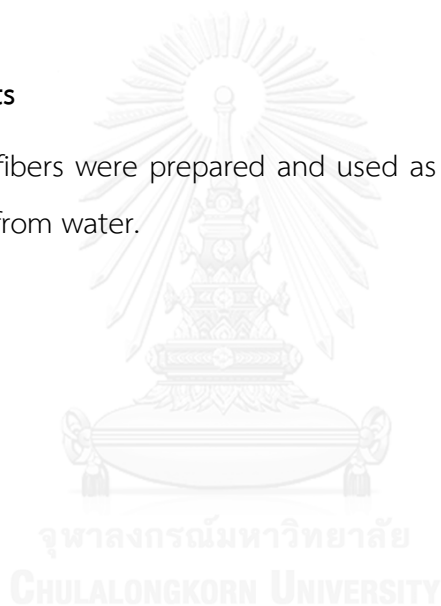
CHAPTER II

THEORY

2.1 ALUMINA

Alumina (Al_2O_3) is one of the most widely used and known as a fine ceramic material. It was applied to the areas of catalysis, reinforcing components, electronic device fabrication, microelectronics, optics, and fire protection [9].

2.1.1 Alumina Structure

Alumina can exist in many metastable phases before transforming to the stable phase (α-alumina; corundum form). There are six metastable phases of alumina chi (χ), kappa (κ), eta (η), theta (θ), delta (δ) and gamma (γ) as shown in Table 2.1. The phase transformation of alumina were conducted by calcined alumina precursors. Difference of the phase transformation sequence is resulted from the different in the precursors structure. In addition, the transformation sequence is irreversible and the final phase of alumina depends on the calcination temperature [10, 11].

Table 2.1 Crystallographic data for transition alumina [12].

Phase	Crystal system
Chi (χ)	Hexagonal
Kappa (κ)	Orthorhombic
Eta (η)	Cubic
Theta (θ)	Monoclinic
Delta (δ)	Monoclinic
Gamma (γ)	Cubic
Alpha (α)	Rhombic

The phase transformation sequence normally starts with aluminium hydroxide (Al(OH)$_3$ and AlOOH). Then, the transformation to low temperature phase of alumina (η and χ) at temperature around 150-500 $^\circ$C is proceeded, and subsequently to high temperature phase (κ, θ, γ and δ) at temperature around 600-1000 $^\circ$C as shown in Figure 2.1. Finally, the stable phase (α), is formed at temperature around 1100-1200 $^\circ$C. However, transition alumina start to lose their surface area at temperature above 800°C due to the elimination of pores and the extreme loss occurs at temperature above 1100 $^\circ$C when the crystallization become to stable α-alumina [13].
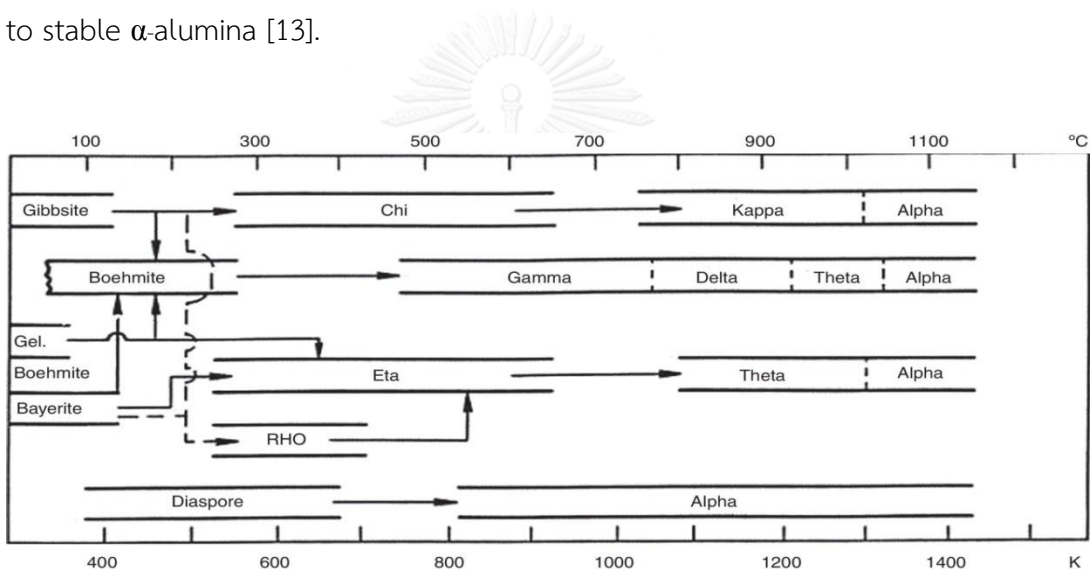
Figure 2.1 Transformation sequence of aluminium hydroxide.

Several researcher [14-16] have been used alumina which rely on gamma and alpha phase due to the γ-alumina having the high surface area and α-alumina having a good mechanical strength. The γ-alumina have widely used as catalyst and catalyst support in the automotive and petroleum industries, such as the use of γ-Al$_2$O$_3$ as a support for Co based catalysts in the Fischer–Tropsch (FT) process for the production of clean fuels [17]. The α-alumina have widely used as reinforcement, such as using α-alumina whiskers as the reinforcing fiber material, and having the resulting polymer nanocomposites superior flexural properties [18].

2.1.2 Preparation of alumina via sol-gel process

Sol is the colloidal suspension of solid particles in the liquid consist of a metal of metalloid element surrounded by various ligands. For example, common precursors for sol-gel synthesis of alumina include inorganic salt such as $Al(NO_3)_3$ and organic compounds such as $Al(OC_4H_9))_3$. The latter is an example of alkoxides, a class of precursors most widely used in sol-gel research [19, 20]. The sol-gel process is shown in Figure 2.2.
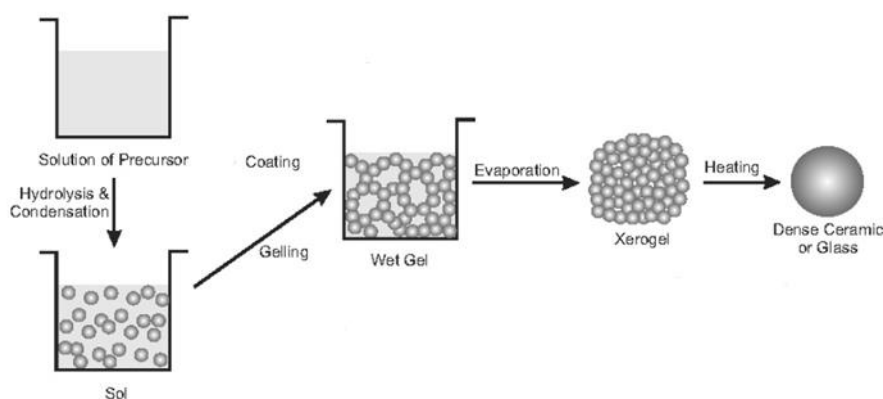
Figure 2.2 the sol-gel process [21].

The chemical and physical properties of the product from sol-gel process are determined by the hydrolysis, condensation and drying steps. The purpose of this process is the transformation of the molecular precursor into a highly crosslinked solid. Hydrolysis leads to a sol, a dispersion of colloidal particles in a liquid, and further condensation results in a gel. Hydrolysis of metal alkoxides M(OR) involves nucleophilic reaction with water. Condensation reactions between two hydroxylated metal species leads to M-O-M bonds under release of water. The reaction is written as follow:

$$M(OR) + H_2O \longleftrightarrow M(OR) + ROH \quad (Hydrolysis)$$

$$M(OR) + M(OR) \longleftrightarrow M\text{-}O\text{-}M + H_2O \quad (Condensation)$$
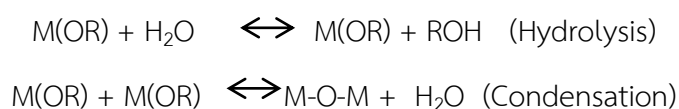
The mechanism of this reaction involves the addition of a negatively charged $HO^{\delta-}$ group to the positively charged metal center ($M^{\delta+}$). The positively charged proton is then transferred to an alkoxy group followed by the removal of ROH. Slow and controlled hydrolysis typically leads to small particles with unique properties. The hydrolysis and condensation rates depend on the electronegativity of the metal atom, the alkoxy group, solvent system, and the molecular structure of the metal alkoxides. Metals with higher electronegativities undergo hydrolysis more slowly than those with lower electronegativity undergo hydrolysis more slowly than those with lower electronegativity. The sensitivity of metal alkoxides toward hydrolysis decreases as size of the OR group increases. Small OR groups lead to high reactivity of the corresponding alkoxide toward water. However, in some cases, high reactivity may result in uncontrolled precipitation of the hydroxide.

The rate of hydrolysis also becomes slow as the coordination number around the metal center in the alkoxide increases. Therefore, alkoxides that tend to form oligomer usually show slower rate of hydrolysis. n-Butoxide is often preferred as a precursor for the synthesis of various oxides because it is the largest alkoxy group that does not prevent oligomerization. For alkoxides with low rate of hydrolysis, acid or base catalyst can be used to enhance the process. The relatively negative alkoxides are protonated by acids creating a better leaving group and eliminating the need for proton transfer in the transition state. Alternatively, bases provide better nucleophile (OH^-) for hydrolysis.

For dying step, dying was achieved by evaporation under normal condition, the gel network shrinks as a result of capillary pressure inside the pores and the product obtained is referred to as xerogel. However, if supercritical drying is applied, the shrinkage of the gel network is reduced, since there is capillary pressure within the pore during drying. Consequently, the pore structure remains largely intact. The product obtained in this manner is referred to as an aerogel [22].

2.2 ELECTROSPINNING

2.2.1 Electrospinning process

Electrospinning process is the process to produce fibers via electric force to draw charged threads of polymer solution or polymer melts up to fibers which have diameters range from nanometers to micrometers. The obtained fibers have good mechanical properties and their surface can be readily modified owing to their high surface area to volume ratio [23] . These fibers are interesting for such application as electrode materials, biomedical application, optical sensor, filter media, sorbent and catalyst support [24, 25] .

The electrospinning process consist of three basic equipments: a high voltage power supply, a spinneret (such as a capillary with metal needle), and a collecting plate (such as metal sheet or rotating mandrel as shown in Figure 2.3. In the electrospinning process, a power supply is connected between anode and cathode [26].
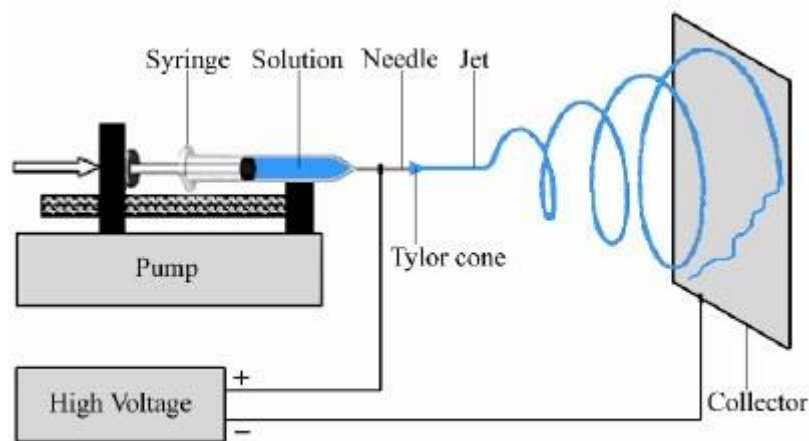
Figure 2.3 Electrospinning process.

At the first stage, voltage is not applied, the surface is the only forces that act on the liquid surface at the outlet of the needle. The shape of the surface is hemispherical in a first approximation. When a positive potential is applied to the

solution at the anode, the hemispherical shape of the solution at the needle will change to Taylor's cone, which is conical shape. The electrical forces overcome the surface tension forces when the electric field applied reaches a critical value. Then, a charged jet of the solution is ejected from the needle of the Taylor cone and a rapid whipping of the jet occurs in the space between the needle and collector which leads to evaporation of the solvent before falling on the collector. The Taylor's cone is shown in Figure 2.4 .
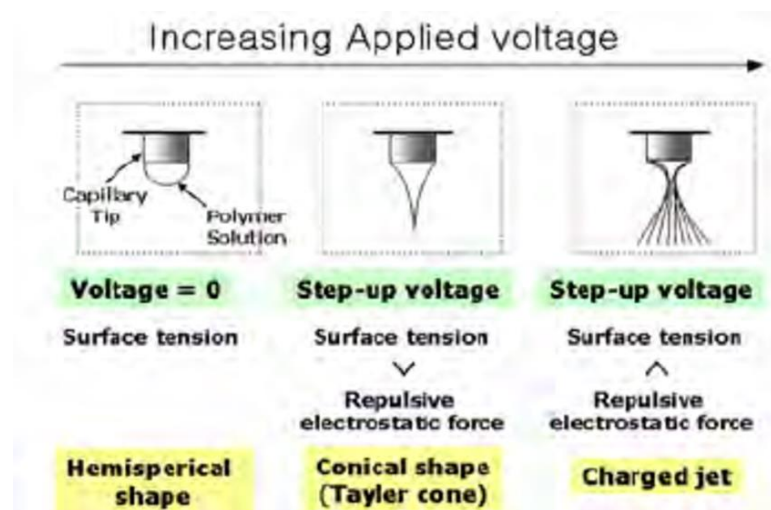
Figure 2.4 Effect of the applied voltage on the formation of the Taylor cone [27].

2.2.2 Parameters of electrospinning

2.2.2.1 Solution concentration

For fibers formation to occur, a minimum solution concentration is required. It has beads found that there should be an optimum solution concentration for the electrospinning process. At low concentrations, beads are formed instead of fibers. As the solution concentration increases, finally uniform fibers with large diameters are formed because of the higher viscosity. At high concentrations, the formation of continuous fibers is prohibited because of the

inability to maintain the flow of the solution at the tip of the needle resulting in the formation of larger fibers.

2.3.2.2 Surface tension

Surface tension is a critical factor in the electrospinning process. The formation of droplets, bead and fibers depend on the surface tension of solution. Reducing the surface tension of the spinning solution, fibers can be obtained without beads, where, the high surface tension prevents the process of spinning owing to instability of the jets and the generation of sprayed droplets.

2.2.2.3 Conductivity

Solution of zero conductivity cannot be an electrospun. Conductivity of spinning solution is mainly determined by the polymer type, solvent used, and additive such as inorganic salt. Increasing of conductivity of the spinning solution, there is a significant decrease in the diameter of the electrospun fibers, whereas, low conductivity of the spinning solution, there results insufficient elongation of a jet by electrical force to produce uniform fibers, and beads may also be observed. However, highly conductive solution are extremely unstable in the presence of strong electric fields which results in a board diameter distribution and beads on the fibers.

2.2.2.4 Applied electric potential

In the electrospinning process, an essential parameter is the applied voltage. After applied voltage, fiber formation will occur, this influence the charges on the solution along with electric field strength will increase the electrostatic repulsive force on the polymer jet. A higher voltage brings about greater stretching of the solution. These effects contribute to reduction in the fiber diameter and also rapid evaporation of the solvent.

2.2.2.5 Collector distance

The distance between the needle and the collector is an important parameter which controls the fibers diameters and morphology because it affects the time spent in the evaporation of the solvent and strength of the electric field. A minimum distance is required to give the sufficient time for fibers to dry before reaching the collector distance, whereas, reducing the collector distance is shorter solven evaporation time, and increase the electric field strength.

2.2.2.6 Flow rate

The flow rate is an important parameter which controls transferring of the polymer from the syringe to the collector. Therefore, a lower feed rate is desirable since the solvent will get enough time for evaporation, and will decrease in diameters of the fibers. Conversely, high flow rates result in bead formation on the fibers owing to unavailability of proper drying time prior to reaching the collector.

2.3 Removal of dye from wastewater

A dye is a colored substance that has an affinity to the substrate to which it is being applied. Dyes are colored because they absorb and reflect light. Organic molecules become colored if they contain at least one of each of the radicals called chromophores and auxochromes. A chromophores containing unsaturated double bonds are the part of a molecule responsible for its color. Moreover, an auxochromes are a functional group of atoms attached to the chromophores which modifies the ability of the chromophores to absorb light and easily soluble in water because of polality [28] .

Dyes are emitted into wastewater from various industries such as dye manufacturing and textile dyeing. Textile wastewater causes several problems when they discharged to environment. In the conventional wastewater treatment consists

of two methods, physicochemical treatment and biological treatment, for removal of dyes from wastewater. However, biological treatments are considered not to be completely adequate. In textile wastewater, there are resistant pollutants to biological degradation, color is reduced but not up to levels that satisfaction. Among the physicochemical treatment techniques for removal of dyes from wastewater, such as chemical coagulation, filtration, oxidation, photocatalytic degradation, and adsorption is the one of the effective techniques that has been employed for dyes removal from wastewater [29, 30] .

2.3.1. Adsorption

Adsorption is the adhesion of atoms, ions, or molecules from a gas, liquid, or dissolved solid to a surface. The solid is known as the adsorbent and the liquid such as dye solution called the adsorbate. This process creates a film of the adsorbate on the surface of the adsorbent [31, 32] .

2.3.1.1 Types of adsorption

Molecules interact with surfaces with forces originating either from the "physical" Van der Waals interaction or from the "chemical" hybridization of their orbitals with those of the atoms of the substrate.

Physical adsorption is relative nonspecific. It is because of the procedure of weak forces of attraction between molecules. Here, the adsorbed molecule is not affixed to a particular site on the solid surface, so it is free to move about over the surface because the surface does not share electrons with the adsorbate. When the molecular forces of attraction between the adsorbate and the adsorbent are greater than the forces of attraction between the adsorbate and the solvent, the adsorbate will be adsorbed onto the adsorbent surface. Physical adsorption is quite reversible. In addition, it has low enthalpy of adsorption (only 20-40 kcal/mole).

Chemical adsorption is the adsorption which involves a chemical reaction which is associated with exchange of electron between the adsorbate and the adsorbent. Then, it has much stronger forces. Regularly the adsorbent form a layer over the surface that is only one molecule thick and the molecules are not considered free to move from one to another site. Chemical adsorption is hardly reversible. In addition, it has high enthalpy of adsorption (20-100 kcal/mole).

2.3.1.2 Adsorption isotherm

Adsorption isotherm is the relation between amount of solute adsorbed per unit mass of adsorbent (Qe) and the equilibrium concentration (Ce). Two well-known adsorption isotherm have been proposed as follows [33, 34] .

Langmuir isotherm

Irving Langmuir was awarded the Nobel Prize in 1932 for his investigations concerning surface chemistry. Langmuir's isotherm describing the Adsorption of adsorbate onto the surface of the adsorbent requires three assumptions: (i) the surface of the adsorbent is in contact with a solution containing an adsorbate which is strongly attracted to the surface, (ii) the surface has a specific number of sites where the solute molecules can be adsorbed and (iii) the adsorption involves the attachment of only one layer of molecules to the surface.

The Langmuir equation can be expressed as equation 2.1.

$$\frac{C_e}{Q_e} = \frac{C_e}{Q_m} + \frac{1}{K_l Q_m} \quad \text{.....equation 2.1}$$

Where C_e (mg/L) is the concentration of dye at equilibrium, Q_e (mg/g) is the amount of dye adsorbed at equilibrium, Q_m (mg/g) is the maximum adsorption capacity and K_l (L/mg) is the Langmuir constant.

Freundlich isotherm

Freundlich isotherm assumes heterogenous surface which is related to the rough surface of the adsorbent. The freundlich isotherm is known equation describing multilayer adsorption. The Freundlich equation can be expressed as equation 2.2.

$$logQ_e = logK_f + \frac{1}{n}logC_e$$ .....equation 2.2

Where C_e (mg/L) is the concentration of dye at equilibrium, Q_e (mg/g) is the amount of dye adsorbed at equilibrium, Q_m (mg/g) is the maximum adsorption capacity, K_f (mg/g $(mg/L)^{1/n}$) is the Freundlich constant and 1/n is related to adsorption intensity.

2.3.2 Photocatalytic degradation

Sunlight is a natural energy source that is abundant and can be exploited for degradation of dye effluent. If we compared to other techniques, then solar light is the best and fast in decolorizing of dye in the presence of metal catalyst. Nano catalysts are widely used for the active removal of dye contaminants. Different type of nano metal oxide (semiconductor) like TiO_2, ZnO and metallic nanoparticles (Au, Ag and Cu) are used for the catalytic degradation of dyes [35-38] .

The primary photocatalytic process occurs upon irradiation of a semiconductor catalyst. A semiconductor is characterized by an electric band structure in which the highest occupied energy band, called valence band, and the lowest band, called conduction band, are separated by band gap. The band gap also defines the wavelength sensitivity of the semiconductor to irradiation. When a photon of the energy higher or equal to the band gap energy is absorbed by a semiconductor, an electron from the valence band is promoted to the conduction band with simultaneous generation of an electronic vacancy or "hole" (h+) in the valence band. Then, donor such as H_2O and acceptor such as oxygen can react with hole and electron to generate hydroxyl radicals ($OH^\bullet$) and superoxide anion (O_2^-) which decomposes organic substance (dyes) by oxidation as shown in Figure 2.5.
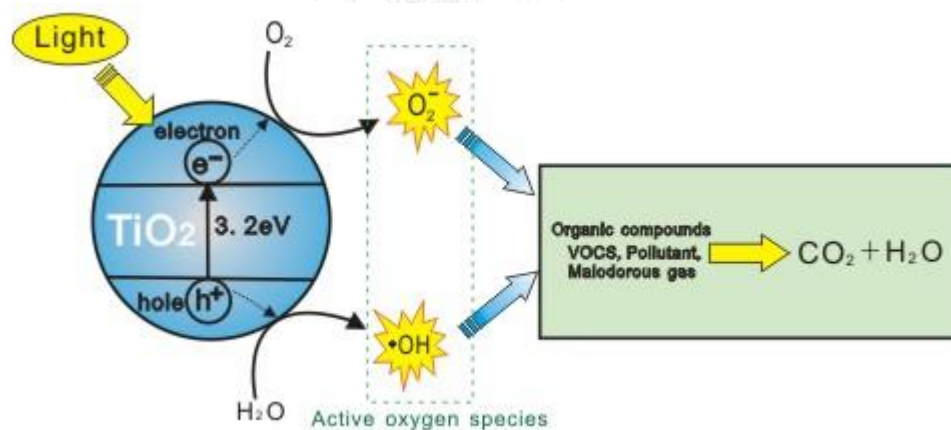
Figure 2.5 The procedure of photocatalytic degradation of organic compounds (dyes) by semiconductor [39].

For the metallic nanoparticles , the photo catalytic properties of metal nanoparticles under the influence of visible light may be well because of excitation of surface plasmon resonance (SPR), which is a oscillation having a charge density that can proliferate at the junction between the dielectric medium and metal surface. Silver nanoparticles have been recently proposed as a novel photocatalyst for degradation of organic pollutants. Since the conduction electrons were excited to higher-energy states, there is a great probability that these electrons can participate in chemical reactions. Simultaneously, the abundant holes left exhibit strong oxidizing power, which can also drive oxidation reactions to achieve photocatalytic degradation of organic compounds as shown in Figure 2.6.
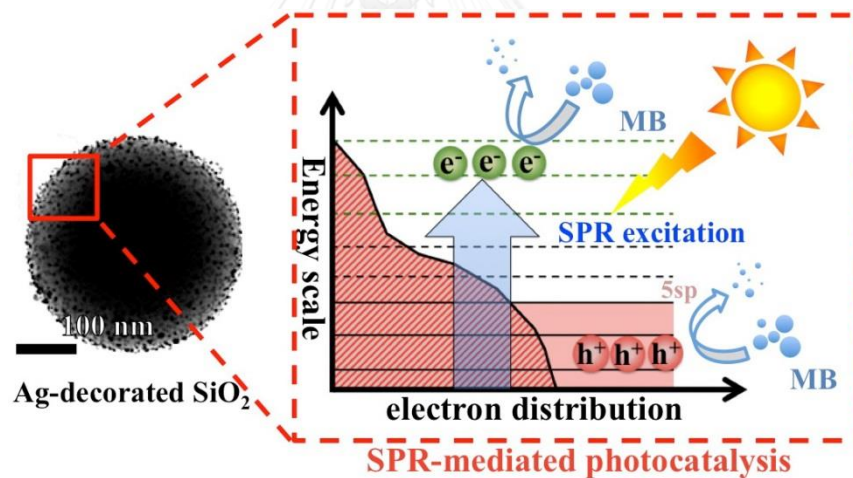
Figure2.6 The procedure of photocatalytic degradation of organic compounds (dyes) by metal nanoparticles [7].

CHAPTER III

EXPERIMENTAL

3.1 Materials

3.1.1 Preparation of fibers

1) Aluminium isopropoxide (98%) (Fisher Scientific Company, USA)

2) Silver nitrate (Avantor Performance Materials, Poland)

3) Polyvinyl alcohol (MW 72,000) (MERCK, Germany)

4) Acetic acid (MERCK, Germany)

5) Ultrapure water (Milli-Q, Millipore, Germany)

3.1.2 Removal of methylene blue experiments

1) Methylene blue (Fisher Scientific Company, USA)

2) Hydrochloric acid (37%) (MERCK, Germany)

3) AvaLight-DHc Light source (Avantes, USA)

4) USB4000-UV-VIS Detector (Ocean Optics, USA)

5) Fiber optic (Ocean Optics, USA)

6) LED 15W (Shining, THA)

3.2 Preparation of adsorbent

3.2.1 Preparation of spinning solution

A typical solution run was as follows: aluminium isopropoxide (AIP) was hydrolyzed with water at 80 $^{\circ}$C under vigorous stirring for 1 h. After that, glacial acetic acid was added to the solution. The molar ratio of AIP/acetic acid/water in final mixed solution was 1:0.15:100. The solution was further stirred at 80 $^{\circ}$C for 18 h in order to form an aluminium hydroxide sol. Then, 2, 4, 6 and 8%w/w of polyvinyl alcohol (PVA) was dissolved in water which is equivalent to the sol solution. Finally, the sol and the PVA solutions were mixed.

3.2.2 Preparation of Al_2O_3 fibers

The electrospinning setup was shown in Figure 3.1. The spinning solution was loaded into a 3-mL plastic syringe that was fitted with a stainless steel needle. High-voltage power supply was connected to the needle and the collector (copper sheet) that was covered with the aluminum foil. During the procedure, the voltage and the flow rate were 21 kV and 0.6 mL/h, respectively. The distance between the needle and the collector was maintained at 16 cm. Finally, the collected fibers called as-spun AIP-PVA fibers, which collected as sheet on the collector were dried in an oven at 110 $^{\circ}$C overnight and calcined at 700 $^{\circ}$C for 3 h in a muffle furnace.
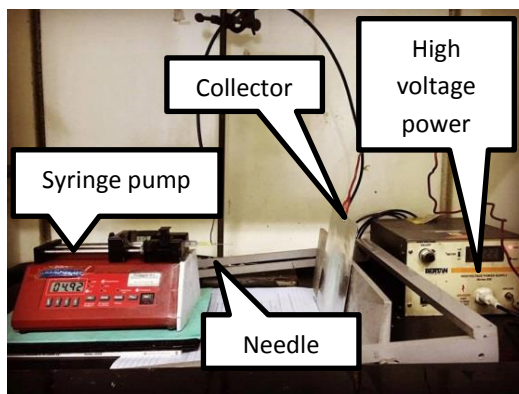
Figure 3.1 Electrospinning setup.

3.2.3 Preparation of Ag/Al$_2$O$_3$ fibers

The Ag/Al$_2$O$_3$ fibers were prepared by conventional impregnation. The Al$_2$O$_3$ fibers was washed with deionized water and discarded by decantation, and then dried in an oven. Afterward, the fibers was immersed in an aqueous solution of silver nitrate to obtain 2, 5 and 10%w/w silver loading and stirred during a 20 hours impregnation period. Then, excess water was evaporated at 80 °C on a hot plate. The solid mass dried at 110 °C overnight and calcined at 350 and 500 °C for 3 hours. The schematic of Ag/Al$_2$O$_3$ fibers preparation were summarized in Figure 3.2.
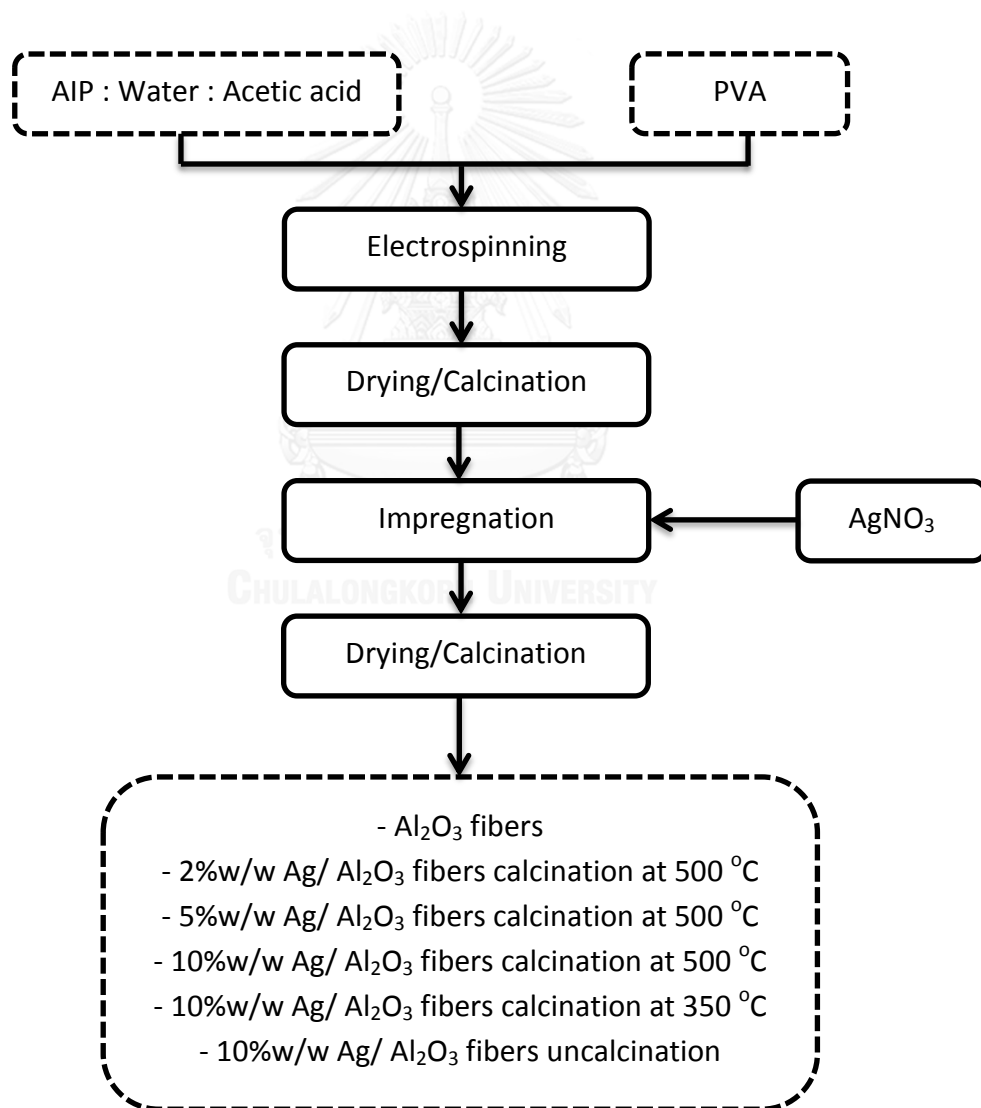
Figure 3.2 A flow chart of the fibers preparation.

3.3 Characterizations of Ag/Al$_2$O$_3$ fibers

3.3.1 Scanning Electron Microscopy (SEM)

The morphology and diameter of the fibers were examined by scanning electron microscopy (SEM, JSM-6610LV) at the Scientific and Technology Research Equipment Centre, Chulalongkorn University (STREC). The average diameter of fibers was measured from SEM images by ImageJ software.

3.3.2 Transmission Electron Microscopy (TEM)

The average diameters of the particles on fibers were examined by transmission electron microscopy (TEM, JEM-2100) at the Scientific and Technology Research Equipment Centre, Chulalongkorn University (STREC) and by transmission electron microscopy (TEM, HITACHI 7700) at Kasetsart Agricultural and Agro-Industrial Product Improvement Institute, Kasetsart University (KAPI). The average diameter of particles on fibers was measured from TEM images by ImageJ software.

3.3.3 Fourier Transform Infrared Spectroscopy (FTIR)

Functional groups in the fibers were identified by using a Fourier transform infrared spectroscopy with ATR mode (FTIR, Nicolet 6700). This unit is located at Analysis Centre of Department of Chemistry, Faculty of Science, Chulalongkorn University.

3.3.4 UV-VIS Spectroscopy

Silver species on the fibers was observed by UV/Vis spectra (Perkin Elmer, Lamda 950) with wavelength ranged from 190 – 700 nm at the Scientific and Technology Research Equipment Centre, Chulalongkorn University (STREC).

3.3.5 X-Ray Diffraction (XRD)

The crystal structure of samples was confirmed by X-ray diffraction (XRD, Rigaku DMAX 2Ultima+) using Cu-Kα radiation and operating at 40 kV and 30 mA. The XRD patterns were collected in 2θ range of 20-80 degree at a scan rate of 5 degree/min. This unit is located at Analysis Centre of Department of Chemistry, Faculty of Science, Chulalongkorn University.

3.3.6 Nitrogen adsorption/desorption

The sorption isotherm and surface area of the fibers were analyzed by surface area analyzer. The characterization is based on the physical adsorption of an inert gas (N_2 adsorption, Microtrac, Belsorp-mini II). The Brunauer-Emmett-Teller (BET) equation from adsorption-desorption isotherms were calculated for the determination of surface area. This unit is located at Analysis Centre of Department of Chemistry, Faculty of Science, Chulalongkorn University. The sample amount of 30 milligrams were dried and outgassed in the sample cell at 200 $^\circ$C for 2 h before adsorption.

3.4 Removal of dye by adsorption process

In these experiments, 3 mg of Ag/Al$_2$O$_3$ fibers was loaded and equilibrated in 3 mL of methylene blue solution under dark condition for 24 hours. The liquid phase was separated from the fibers by centrifugation at 3500 rpm for 5 minutes. The concentration of methylene blue in the solution was analyzed by UV-Vis spectrophotometry at 660 nm. The UV-Vis spectrophotometry setup was shown in Figure 3.3.
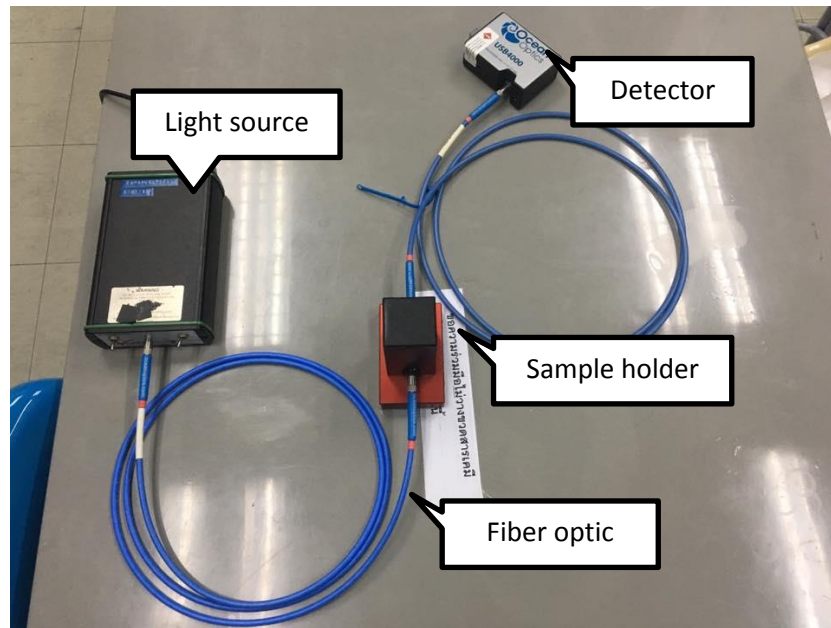
Figure 3.3 UV-Vis spectrophotometry setup.

The removal efficiency of methylene blue by adsorption process was calculated using the relationship described as follows:

Dye removal (%) = $((C_0 - C_e) / C_0) \times 100$

Where, C_0 (mg/L) and C_e (mg/L) are the initial dye concentration and the equilibrium concentration, respectively.

The amount of dye uptake by the fibers was calculated using as follows:

$Q_e = (C_0 - C_e) \times V/M$

Where, Q_e (mg/g) is the amount of dye loaded on per unit of adsorbent at equilibrium; V (L) volume of dye solution and M (g) mass of the adsorbent used.

3.4.1 Adsorption capacity of Ag/Al_2O_3 fibers

A various initial concentration of methylene blue is investigated to predict maximum adsorption capacity (Q_m) using Langmuir's isotherm. The fibers and 2, 5, 8 and 10 mg/L methylene blue with a pH of 6.6 was taken in 20 mL vial bottle. The methylene blue solutions were taken after adsorption process.

3.4.2 pH of dye solution

The fibers and 10 mg/L methylene blue with a pH of 2, 4 and 6 was taken in 20 mL vial bottle. The pH of the solution was adjusted using HCl. The methylene blue solutions were taken after adsorption process.

3.5 Removal of dye by photocatalytic degradation

Photocatalytic degradation of methylene blue is investigated to determine removal efficiency by photocatalytic reaction and compare with the kinetic model. The fibers and 10 mg/L of methylene blue solution with a pH of 6.6 was taken in 20 mL vial bottle. Once the dye adsorption equilibrium is reached, the mixture was illuminated by sun light during 12.00 – 15.00 pm of the day and by a 15 W LED lamp. The methylene blue solutions were taken in an equal time of 100 min.

3.6 Reusability

The fibers which were used in section 3.5 were isolated from the dye solution. The collected spent fibers were dried overnight at 80 $^{\circ}$C in hot-air oven and washed with distilled water. Then, the fibers were isolated and oven dried again. The reusability of the fibers was determined by performing experiments repetitively three times.

CHAPTER IV

RESULTS AND DISCUSSION

This chapter is separated into two parts which are the characterization of prepared Ag/Al_2O_3 fibers and the activity of Ag/Al_2O_3 fibers for removal of methylene blue.

4.1 Characterizations of Ag/Al_2O_3 fibers

4.1.1 Scanning Electron Microscopy (SEM)
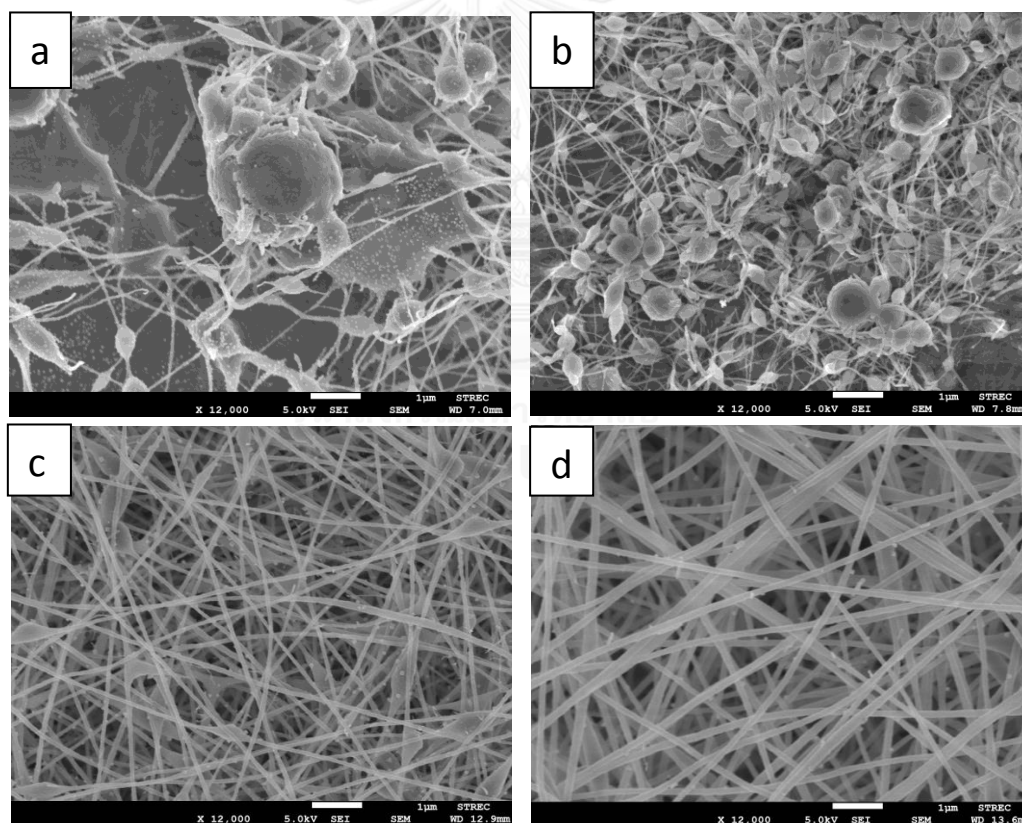
Figure 4.1 SEM images of as-spun AIP/PVA fibers with (a) 2 (b) 4 (c) 6 and (d) 8%w/w PVA.

Figure 4.1 shows the SEM images of as-spun AIP/PVA fibers at various PVA concentrations (2, 4, 6 and 8%w/w). The concentrations of PVA largely affected the morphology of the fibers resulting from the change of viscosity of the spinning solution. The morphology and diameter of fibers were summarized in Table 4.1.

Table 4.1 Morphology of fibers at various PVA concentrations.

Fibers	PVA concentration (%w/w)	Fiber morphology	Average diameter (nm)
as-spun AIP/PVA	2	Fibers with bead	63
as-spun AIP/PVA	4	Fibers with bead	68
as-spun AIP/PVA	6	Bead-liked fibers	84
as-spun AIP/PVA	8	Fine fibers	124
Al_2O_3	8	Irregular fibers	75

The as-spun AIP/PVA fibers with 2 and 4%w/w of PVA result fibers with bead. (Figure 4.1a and 4.1b) relating to low viscosity of PVA solution. The as-spun AIP/PVA fibers with 6%w/w of PVA (Figure 4.1c) result a better fiber but still have beads on fibers. The smooth and regular form of the as-spun AIP/PVA fibers were produced with 8%w/w of PVA (Figure 4.1d) resulting from the increase of the viscosity of the spinning solution. The obtained fibers with 8%w/w of PVA have average diameter of 124 nm. However, after calcined these as-spun AIP/PVA fibers, Al_2O_3 fibers (Figure 4.2) was irregular and rough surface. In addition, the diameters of the Al_2O_3 fibers were 75 nm which were smaller than as-spun AIP-PVA fibers. It caused by the removal of PVA and the growth of alumina grains within fibers. Al_2O_3 fibers with 8%w/w of PVA were fabricated and studied in further experiments.
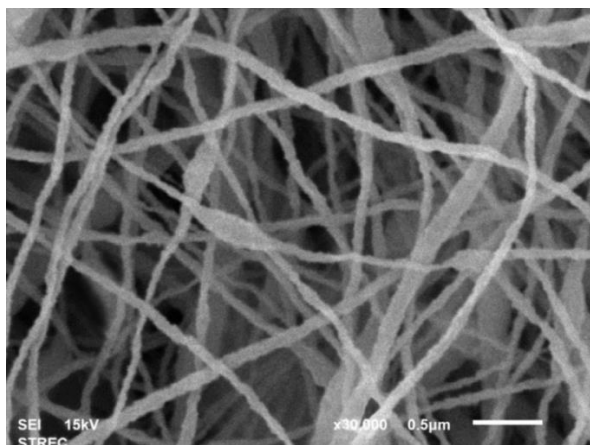
Figure 4.2 SEM images of Al$_2$O$_3$ fibers with 8%w/w of PVA.

4.1.2 Transmission Electron Microscopy (TEM)

Figure 4.3 shows TEM images of Ag/Al$_2$O$_3$ fibers at various silver concentrations (2, 5 and 10%w/w) and Figure 4.4 shows TEM images of Ag/Al$_2$O$_3$ fibers at different calcination temperatures. The average particle diameter of the silver were summarized in Table 4.2.

Table 4.2 Particle diameter of the silver at various silver concentrations and different calcination temperatures.

Fibers	Particle size (nm)
2%w/w Ag/Al$_2$O$_3$ fibers (500 $^\circ$C calcination)	3
5%w/w Ag/Al$_2$O$_3$ fibers (500 $^\circ$C calcination)	5
10%w/w Ag/Al$_2$O$_3$ fibers (500 $^\circ$C calcination)	13
10%w/w Ag/Al$_2$O$_3$ fibers (350 $^\circ$C calcination)	11
10%w/w Ag/Al$_2$O$_3$ fibers (uncalcination)	7
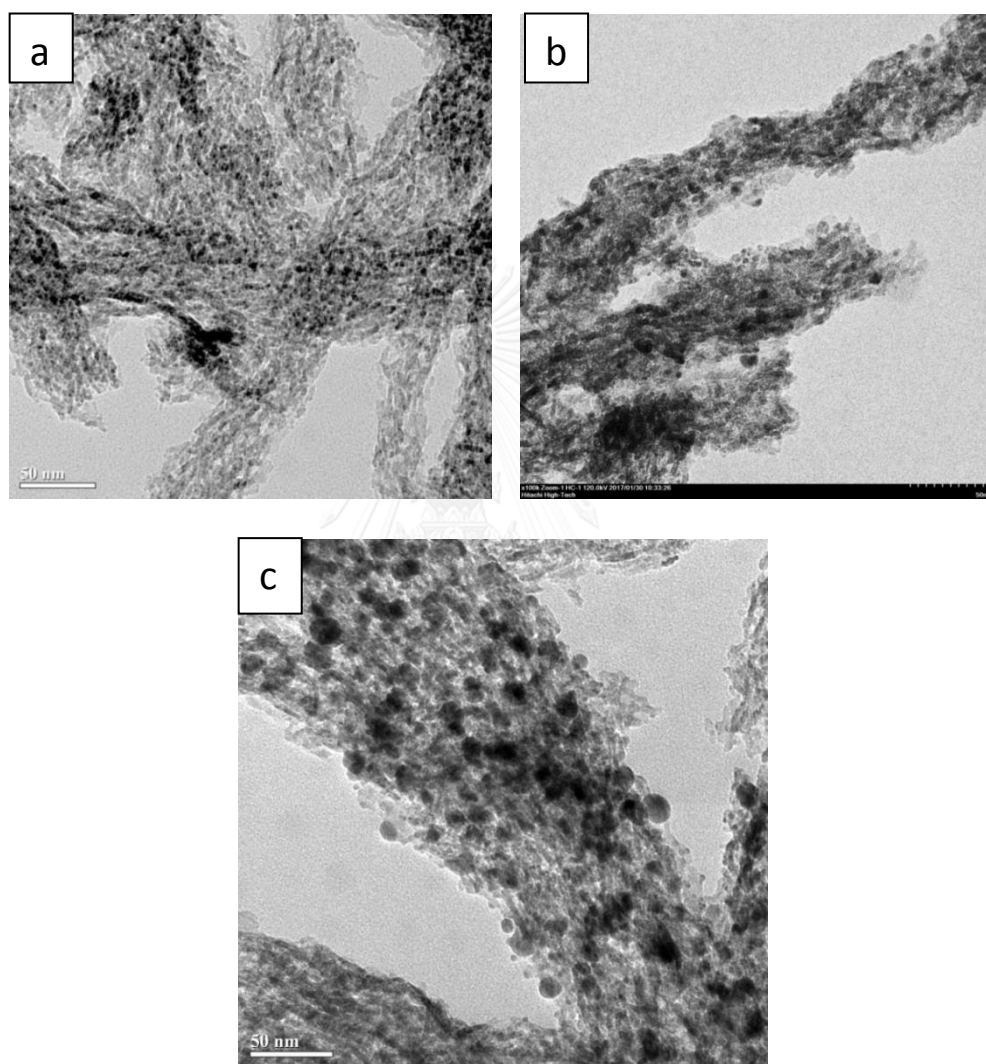
Figure 4.3 TEM images of Ag/Al$_2$O$_3$ fibers after calcination at 500°C with various Ag

concentations: (a) 2%w/w (b) 5%w/w (c) 10%w/w.
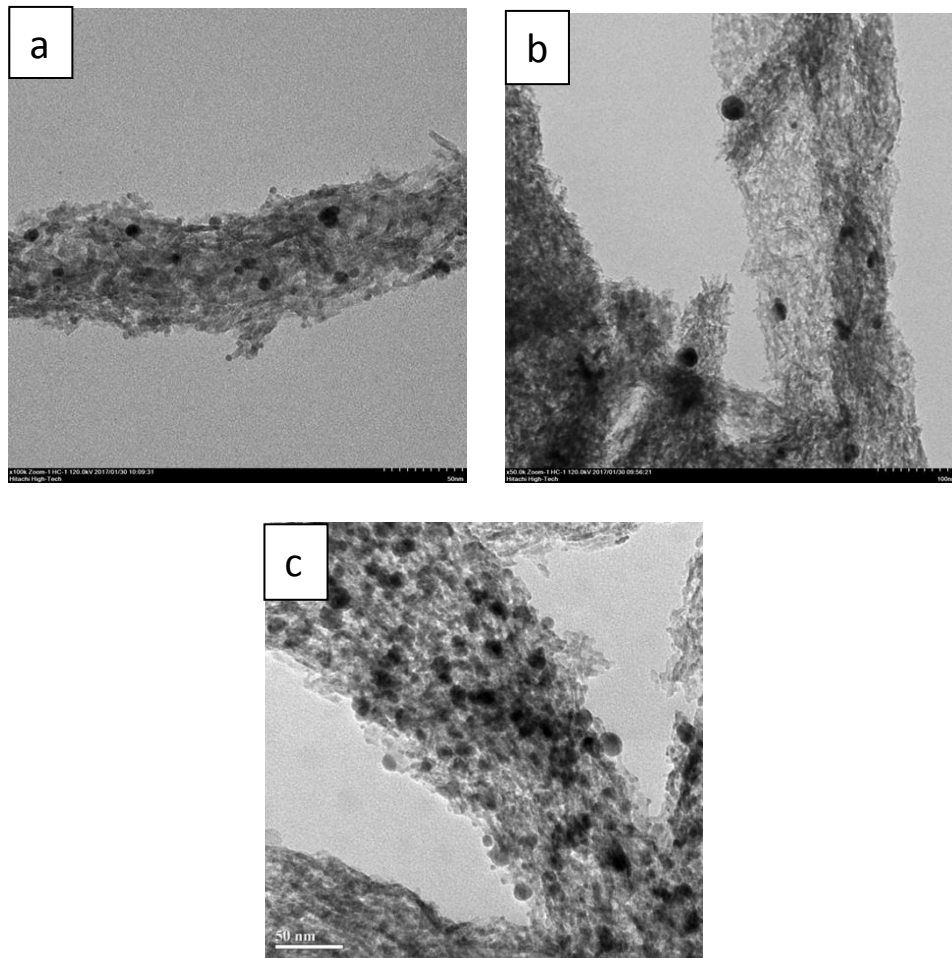
Figure 4.4 TEM images of Ag/Al$_2$O$_3$ fibers with 10% w/w Ag
at: (a) uncalcined (b) calcination at 350°C (c) calcination at 500°C.

In Figure 4.3 and 4.4, dark spots in the TEM images implied silver particles exhibited in the Al$_2$O$_3$ crystal. The silver particles in Al$_2$O$_3$ fibers were observed and the size of silver particles was increased with increasing a concentration of silver source (silver nitrate salt) because of agglomeration. It is observed that the particles size of silver increase from 3 to 13 nm. Moreover, by comparing uncalcined 10%w/w Ag/Al$_2$O$_3$ fibers and calcined 10%w/w Ag/Al$_2$O$_3$ fibers at 350 and 500 $^{\circ}$C, the amount of Ag particle in the Ag/Al$_2$O$_3$ fibers were increased. Evidently, the calcination temperature promoted the production of Ag particle. However, the particles size of silver increase from 7 to 13 nm.

4.1.3 Fourier Transform Infrared Spectroscopy (FTIR)
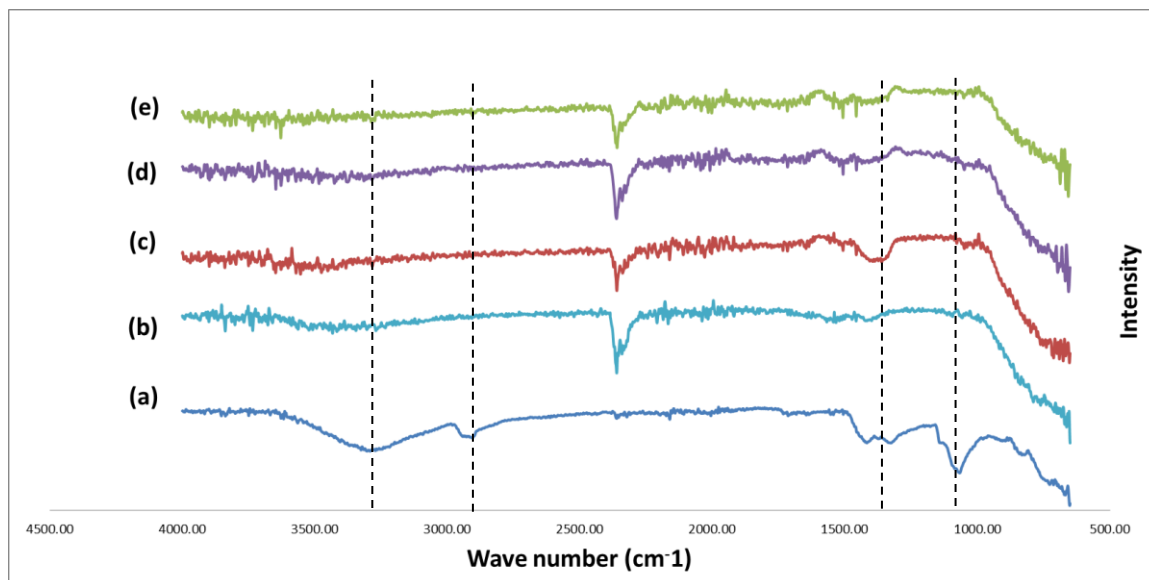
Figure 4.5 FTIR spectra of (a) as-spun AIP/PVA fibers, (b) Al_2O_3 fibers and 10%w/w Ag/Al_2O_3 fibers after calcination at (c) uncalcination (d) 350 $^{\circ}$C (e) 500 $^{\circ}$C.

Figure 4.5 shows the FTIR spectra of the uncalcined 10%w/w Ag/Al_2O_3 fibers and calcined Ag/Al_2O_3 fibers at 350 and 500 $^{\circ}$C, the as-spun AIP/PVA fibers and Al_2O_3 fibers. The Ag/Al_2O_3 fibers with different concentrations of silver were not studied because silver particles did not respond to the infrared spectra. The characteristic absorption bands of PVA were observed in as-spun AIP/PVA fibers, which are 3278 cm^{-1} (stretching of OH), 2935 cm^{-1} (asymmetric stretching of CH_2), 2906 cm^{-1} (symmetric stretching of CH_2), 1325-1417 cm^{-1} (wagging of CH_2 and bending of OH), 1143 cm^{-1} (stretching of CO from crystalline sequence of PVA), and 1088 (stretching of CO and bending of OH from amorphous sequence of PVA). The characteristic peaks of PVA were not observed in Al_2O_3 and Ag/Al_2O_3 fibers. It was confirmed that PVA is an assisting agent in the electrospinning process and decomposed after calcination of Al_2O_3 fibers. The γ-Al_2O_3 characteristic bands were

observed in the range between 600-800 cm^{-1} (stretching of Al-O) and the weak band at around 3200 - 3600 cm^{-1} indicating the presence of Al-OH bonds in these fibers. The other bands are around 2350 cm^{-1} which attributed to the presence of some undesired impurities in γ-Al$_2$O$_3$ [40] .The absorption band at 1385 cm^{-1} referred to a stretching of NO was observed for uncalcined 10%w/w Ag/Al$_2$O$_3$ fibers but none of this band in calcined Ag/Al$_2$O$_3$ fibers. It indicated that AgNO$_3$ residues were precipitated on the surface of alumina after impregnation process and decomposed after calcination at 350 and 500 $^{\circ}$C.

4.1.4 UV-VIS Spectroscopy

UV/Vis spectra were taken to observe the details of the state of the silver species. The absorbance at 215 nm and 320 nm assigned to dispersed Ag^{+} ions and Ag$_n^{\delta+}$ clusters which incorporated within the alumina-oxygen coordinated structure, respectively. The absorbance above 320 nm is due to the existence of the Ag^0 particles [41]. Figure 4.6 shows the UV/Vis spectra of the Al$_2$O$_3$ fibers and Ag/Al$_2$O$_3$ fibers at various silver concentrations (2, 5 and 10%w/w). It was indicated that the amount of Ag^{+}, Ag$_n^{\delta+}$ and Ag^0 species in Ag/Al$_2$O$_3$ fibers were similar in response to alteration of silver loading and the Al$_2$O$_3$ fibers showed little absorbance in the range of 190-700 nm.
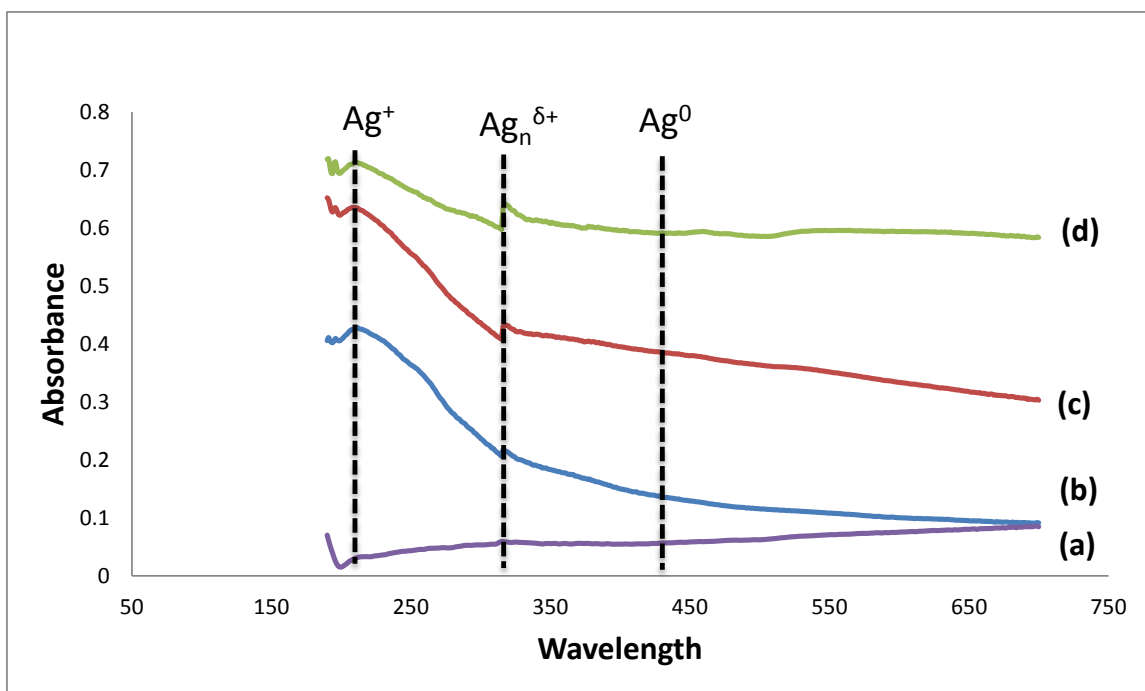
Figure 4.6 UV/Vis spectra of (a) Al_2O_3 fibers and Ag/Al_2O_3 fibers with (b) 2 %w/w (c) 5 %w/w (d) 10%w/w of silver (calcination at 500 $^\circ$C).
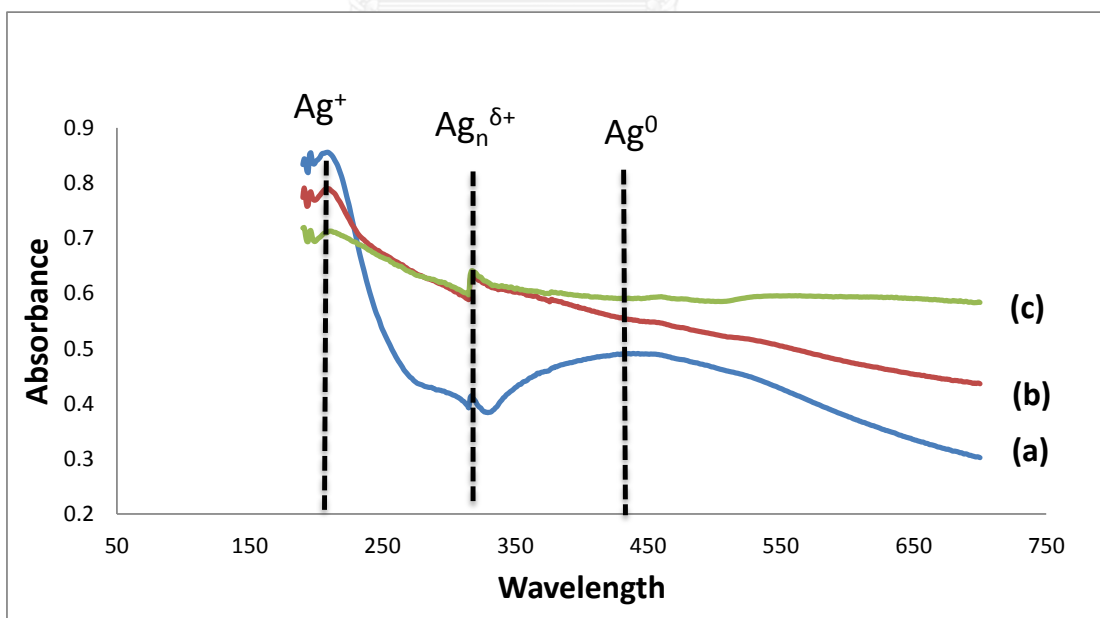
Figure 4.7 UV/Vis spectra of 10%w/w Ag/Al_2O_3 fibers (a) uncalcination (b) calcination at 350 $^\circ$C (c) calcination at 500 $^\circ$C.

Figure 4.7 shows the UV/Vis spectra of the uncalcined and calcined Ag/Al_2O_3 fibers at 350 and 500 ^{o}C. The results show that uncalcined Ag/Al_2O_3 fibers have a lower absorbance at the region of both $Ag_n^{\delta+}$ clusters and Ag^0 particles than the calcined Ag/Al_2O_3 fibers. It is because uncalcined Ag/Al_2O_3 fibers still have $AgNO_3$ which is related to the result from FTIR spectra. However, by comparing between calcined Ag/Al_2O_3 fibers at 350 and 500 ^{o}C, the calcined Ag/Al_2O_3 fibers at 500°C show slightly higher absorbance at the region of Ag^0 particles.

4.1.5 X-Ray Diffraction (XRD)

XRD spectra were taken to observe the details of the phase identification of a crystalline of the fibers. Figure 4.8 and 4.9 show the XRD spectra of the as-spun AIP/PVA fibers, Al_2O_3 fibers and Ag/Al_2O_3 fibers at various silver concentrations (2, 5 and 10%w/w). Although the as-spun AIP/PVA fibers still have a polymer in the fibers which are not decomposed, the pattern of as-spun AIP/PVA fibers indicates boehmite instead of amorphous nature of polymer. The γ-Al_2O_3 pattern is evident when the fibers are calcined and the boehmite pattern disappears. These results imply that the boehmite transform into crystalline alumina. The peaks corresponding to Ag^0 particles were observed in the spectra of 5 and 10%w/w Ag/Al_2O_3 fibers. Especially, the 10%w/w Ag/Al_2O_3 fibers have had the strong Ag^0 particles diffraction peak due to the large amount of Ag^0 particles, whereas no Ag^0 particles were remarked in the spectra of 2%w/w Ag/Al_2O_3 fibers. It might be because of too small amount of metallic silver to detect by X-ray diffraction.
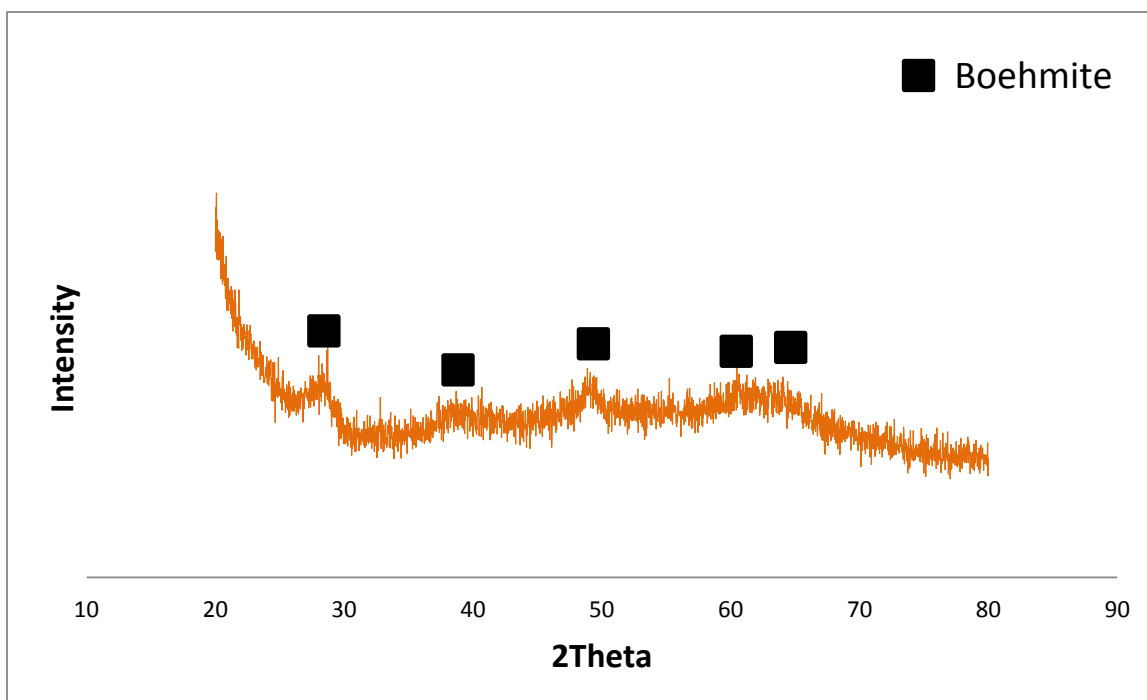
Figure 4.8 XRD spectra of as-spun AIP/PVA fibers.
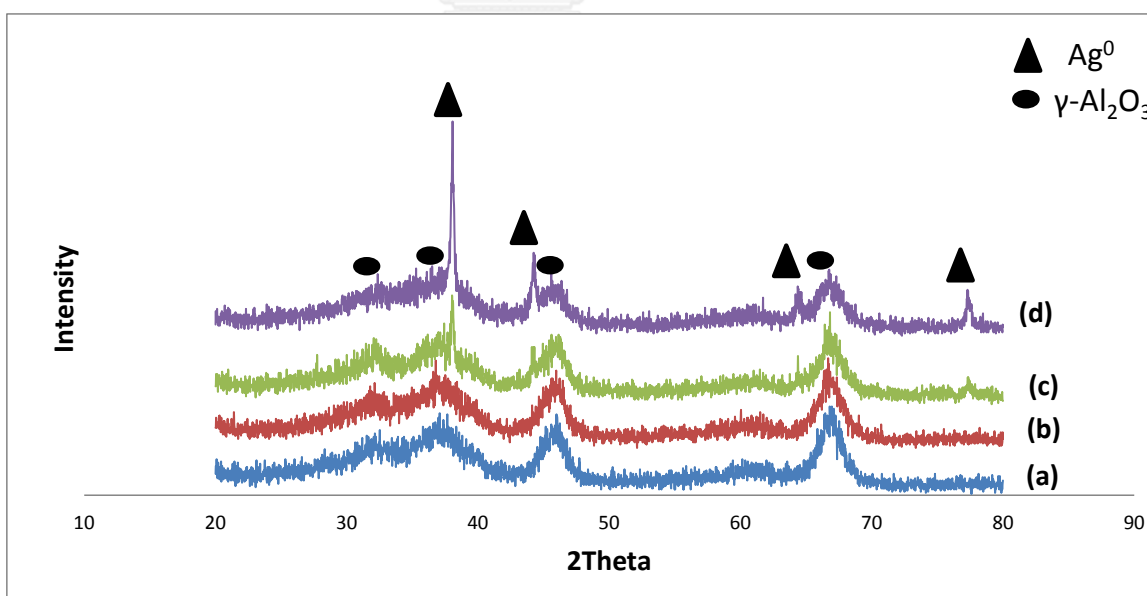
Figure 4.9 XRD spectra of (a) Al_2O_3 fibers and Ag/Al_2O_3 fibers calcination at 500 $^{\circ}$C with (b) 2%w/w (c) 5%w/w (d) 10%w/w of silver.
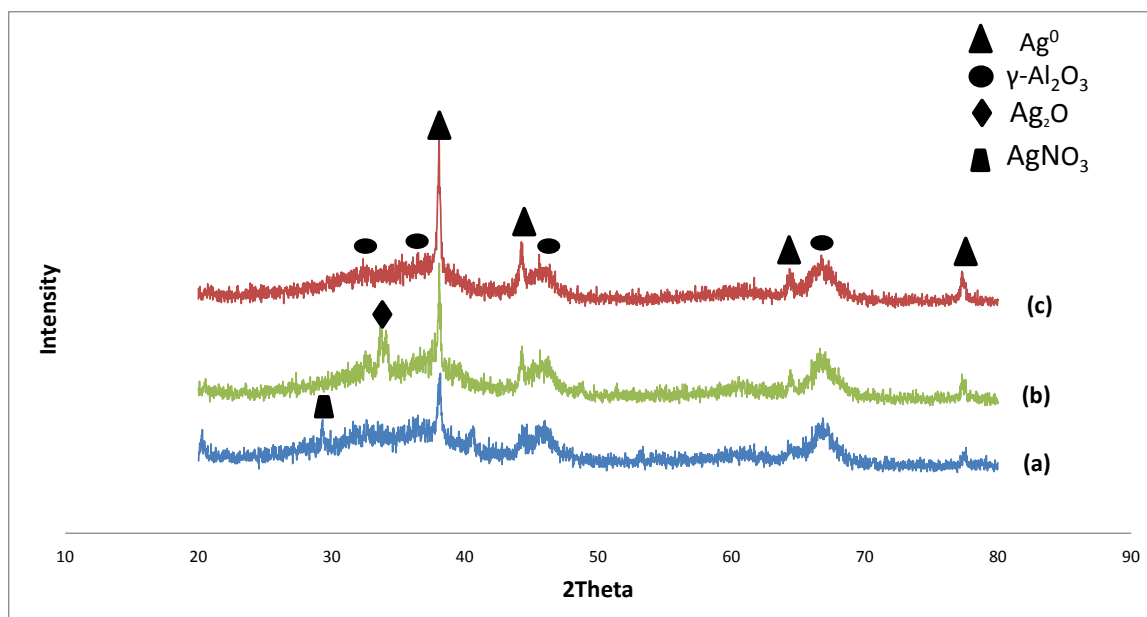
Figure 4.10 XRD spectra of 10%w/w Ag/Al$_2$O$_3$ fibers (a) uncalcination (b) calcination at 350 $^{\circ}$C (c) calcination at 500 $^{\circ}$C.

Figure 4.10 shows the XRD spectra of the uncalcined and calcined 10%w/w Ag/Al$_2$O$_3$ fibers at 350 and 500 $^{\circ}$C. All of the samples show that peaks can be indexed to the structure of Ag^0 particles. For the uncalcined 10%w/w Ag/Al$_2$O$_3$ fibers, the peak of Ag^0 particles is weak by comparing to the others and the peaks of AgNO$_3$ are also observed. These results confirmed that AgNO$_3$ was precipitated on the surface of alumina as described in the result of FTIR spectra and some of metallic silver is occurred as described in the result of UV/Vis spectra. Surprisingly, the peaks of Ag$_2$O are observed in calcined 10%w/w Ag/Al$_2$O$_3$ fibers at 350 $^{\circ}$C. It is probably due to thermal treatment under oxidative (O$_2$) atmosphere. Some of Ag^0 particles react with oxygen to form Ag$_2$O particles. However, at high temperature, Ag$_2$O might be decomposed to form Ag^0 particles as shown in calcined 10%w/w Ag/Al$_2$O$_3$ fibers at 500 $^{\circ}$C XRD spectra.

4.1.6 Nitrogen adsorption/desorption
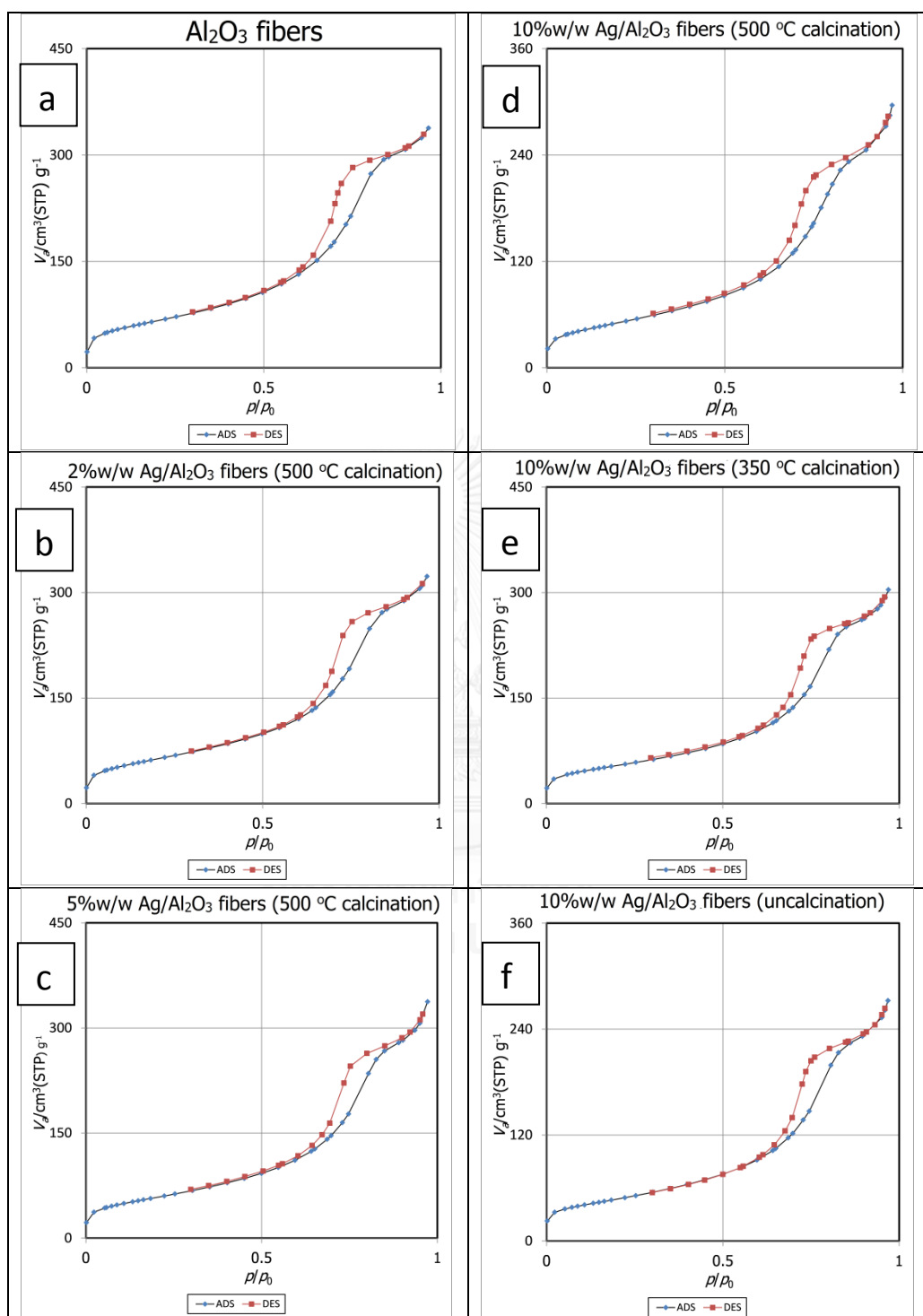
Figure 4.11 Nitrogen adsorption-desorption isotherms of (a) Al_2O_3 fibers (b) 2%w/w Ag/Al_2O_3 fibers (500 $^\circ$C calcination) (c) 5%w/w Ag/Al_2O_3 fibers (500 $^\circ$C calcination) (d) 10%w/w Ag/Al_2O_3 fibers (500 $^\circ$C calcination) (e) 10%w/w Ag/Al_2O_3 fibers (350 $^\circ$C calcination) (f) 10%w/w Ag/Al_2O_3 fibers (uncalcination).
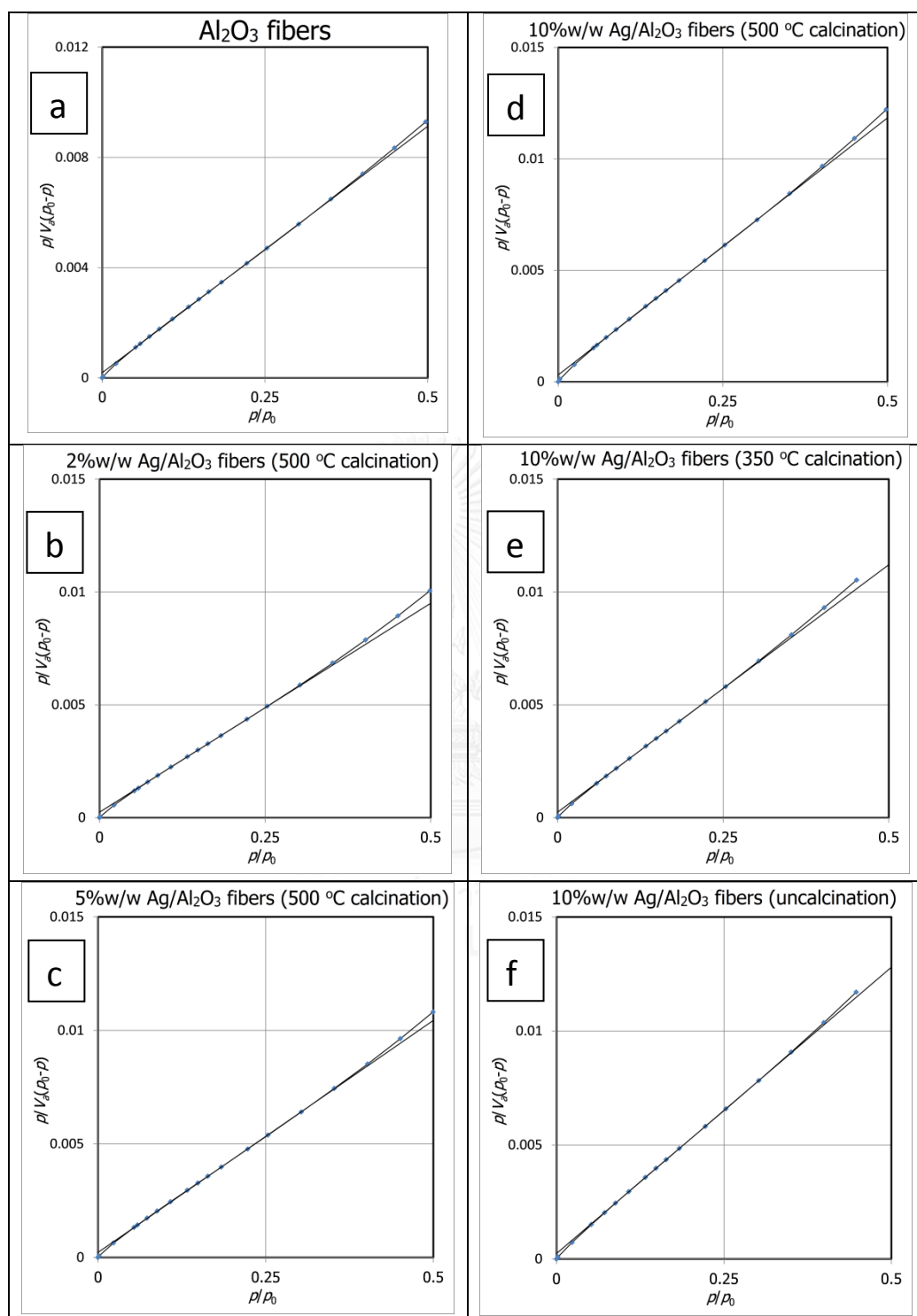
Figure 4.12 BET-Plots of of (a) Al_2O_3 fibers
(b) 2%w/w Ag/Al_2O_3 fibers (500 $^\circ$C calcination) (c) 5%w/w Ag/Al_2O_3 fibers (500 $^\circ$C calcination) (d) 10%w/w Ag/Al_2O_3 fibers (500 $^\circ$C calcination) (e) 10%w/w Ag/Al_2O_3 fibers (350 $^\circ$C calcination) (f) 10%w/w Ag/Al_2O_3 fibers (uncalcination).

In Figure 4.11, all the nitrogen adsorption-desorption isotherms of the Al_2O_3 fibers and Ag/Al_2O_3 fibers show a type IV of porous materials following the IUPAC (International Union of Pure and Applied Chemistry) that is a characteristics of mesoporous. In mesoporous materials more number of molecules interacts with each other due to larger pores, and consequently, enhance catalytic properties. The shape of hysteresis loop (type H4) formed by capillary condensation indicates that some mesopores exist in the slits of the fibers. The type IV isotherm [42] is presented to adsorption that related to Brunauer-Emmett-Teller (BET) method for calculation of specific surface, pore size and pore volume on the fibers. Therefore, the nitrogen adsorption-desorption isotherms were well fitted to BET-Plot as shown in Figure 4.12. Surface area, pore diameter and total pore volume calculated from BET-plot were summarized in Table 4.3.

Table 4.3 BET results of the fibers.

Fibers	Surface area (m^2/g)	Mean pore diameter (nm)	Total pore volume (cm^3/g)
Al_2O_3 fibers	240	8.68	0.52
2%w/w Ag/Al_2O_3 fibers (500 $^\circ$C calcination)	231	8.61	0.49
5%w/w Ag/Al_2O_3 fibers (500 $^\circ$C calcination)	210	9.84	0.52
10%w/w Ag/Al_2O_3 fibers (500 $^\circ$C calcination)	186	9.91	0.46
10%w/w Ag/Al_2O_3 fibers (350 $^\circ$C calcination)	196	9.58	0.47
10%w/w Ag/Al_2O_3 fibers (uncalcination)	171	9.81	0.42

From Table 4.3, the highest surface area was observed in Al_2O_3 fibers. For the Ag/Al_2O_3 fibers at various silver concentrations (2, 5 and 10%w/w), the Ag/Al_2O_3 fibers surface area is lower than that of their respective host material from 240 to 186 m^2/g. However, mean pore diameter show slightly increased from 8.68 to 9.91 nm and pore volume is not changed much. It is speculated that the lower surface area and larger mean pore diameter on the Ag/Al_2O_3 fibers related towards the presence of some bulk particles which blocked the smaller pores and thus shifting the pore size. For the uncalcined and calcined 10%w/w Ag/Al_2O_3 fibers at 350 and 500 $^{\circ}$C, the uncalcined 10%w/w Ag/Al_2O_3 fibers show the lowest surface area. It is probably due to the deposition of $AgNO_3$ which may be blocking pore mouths and not dissolving in the solid matrix. However, the calcined 10%w/w Ag/Al_2O_3 fibers at 350 $^{\circ}$C show higher surface area than the calcined 10%w/w Ag/Al_2O_3 fibers at 500 $^{\circ}$C. It is because of the calcined 10%w/w Ag/Al_2O_3 fibers at 500 $^{\circ}$C have the larger particles which deposit on the surface of alumina as shown in the results of TEM. However, mean pore diameter and pore volume are not changed much.

4.2 Removal of dye

In this study, methylene blue is used to examine the capability of Ag/Al_2O_3 for dye removal. Al_2O_3 fibers with 2, 5, and 10 %w/w Ag/Al_2O_3 fibers calcined at 500 $^{\circ}$C were denoted as 0Ag, 2Ag, 5Ag, and 10Ag, respectively. Moreover, 10 %w/w Ag/Al_2O_3 fibers calcined at 350 $^{\circ}$C and uncalcined were denoted as 10Ag350 and 10AgU, respectively.

4.2.1 Adsorption capacity of Ag/Al$_2$O$_3$ fibers
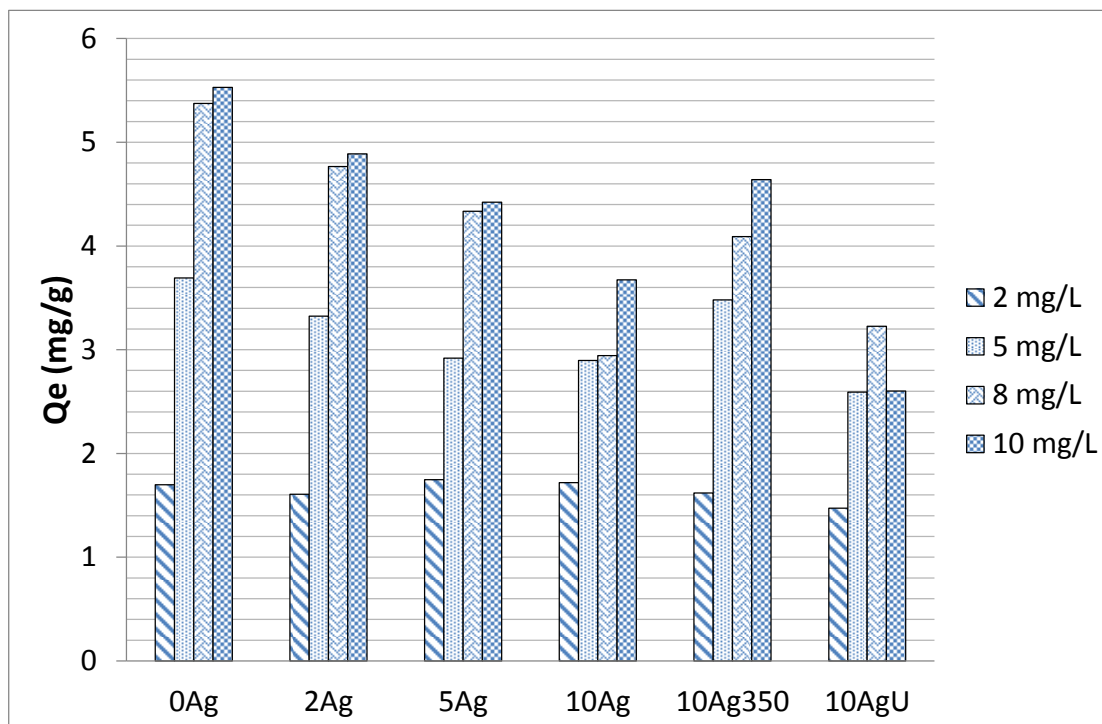
Figure 4.13 Effect of initial concentrations on the adsorption of methylene blue.

The adsorption capacity was evaluated by varied the initial dye concentrations in the range of 2 to 10 mg/L of methylene blue. Figure 4.13 shows the amount of dye loaded on per unit of adsorbent (Q$_e$) at equilibrium. For all of the samples except uncalcined 10 %w/w Ag/Al$_2$O$_3$ fibers, the amount of dye loaded on per unit of adsorbent increasing when the initial methylene blue concentrations are increased. Indeed, at higher initial concentrations, the resistance to mass transfer between the solid and aqueous phase is more easily overcome due to the driving forces. In addition, the number of collisions between dye molecules and adsorbent increases. However, the uncalcined 10 %w/w Ag/Al$_2$O$_3$ fibers showed the highest amount of dye loaded on per unit of adsorbent at 8mg/L and decreased when the initial dye concentration is 10 mg/L. It might be because the available adsorption sites of the fibers were reached the limit at this condition.

The maximum amount of dye loaded on per unit of adsorbent (Q_m) was examined from the adsorption isotherm. Table 4.4 summarized the R^2 of the Langmuir and Freundlich isotherms equation. The results showed that the Langmuir isotherm fitted the experimental data better than the Freundlich isotherm. Then, the Langmuir equation was used to predict the Q_m of the fibers on the adsorption of methylene blue and compared in Figure 4.14.

Table 4.4 R^2 of the adsorption isotherm.

Fibers	Langmuir	Freundlich
	R^2	R^2
0Ag	0.9905	0.9764
2Ag	0.9891	0.9687
5Ag	0.9602	0.9565
10Ag	0.9647	0.9337
10Ag350	0.994	0.9495
10AgU	0.9669	0.7932
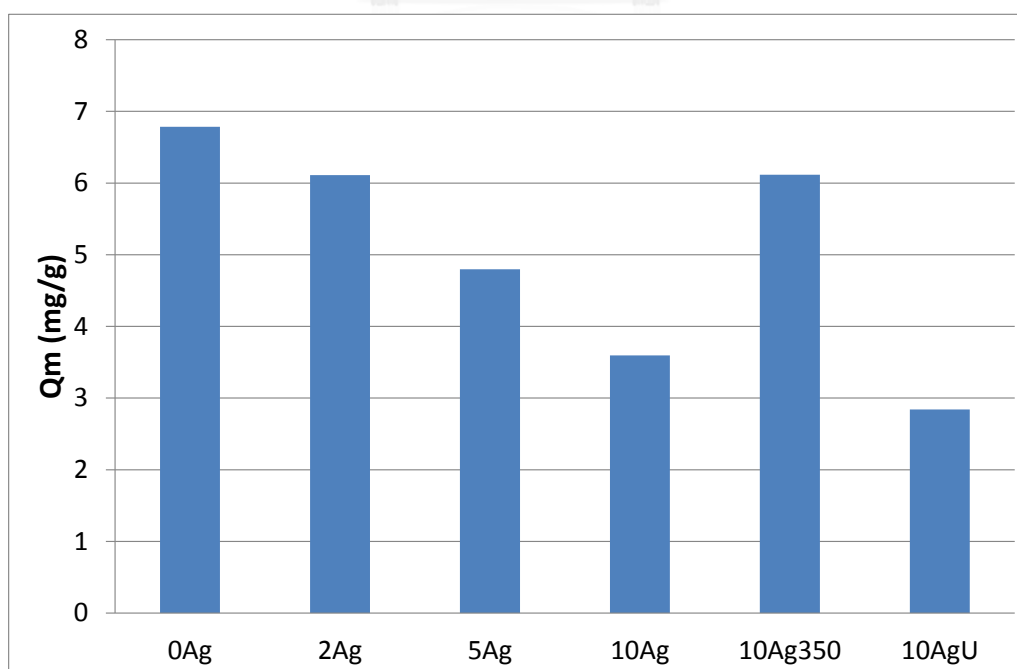
Figure 4.14 Maximum capacity for the adsorption of methylene blue.

From Figure 4.14 even though many researchers reported that silver is favorable for the adsorption of sulfur compound, the results revealed that the adsorption capacity of all fibers except calcined 10%w/w Ag/Al_2O_3 fibers at 350 $^{\circ}C$ is decreased from 6.8 to 2.8 mg/g. These results indicate that the adsorption of methylene blue is overcome by alumina adsorption which is related to the results of BET surface area. On the contrary, the adsorption capacity with calcined 10%w/w Ag/Al_2O_3 fibers at 350 $^{\circ}C$ is up to 6.1 mg/g. This observation implies that Ag_2O particles, which observed in the calcined 10%w/w Ag/Al_2O_3 fibers at 350 $^{\circ}C$, play an important role in the adsorption of methylene blue. It might probably due to the sulfur compound is more favorable to interact with Ag_2O.

4.2.2 pH of dye solution
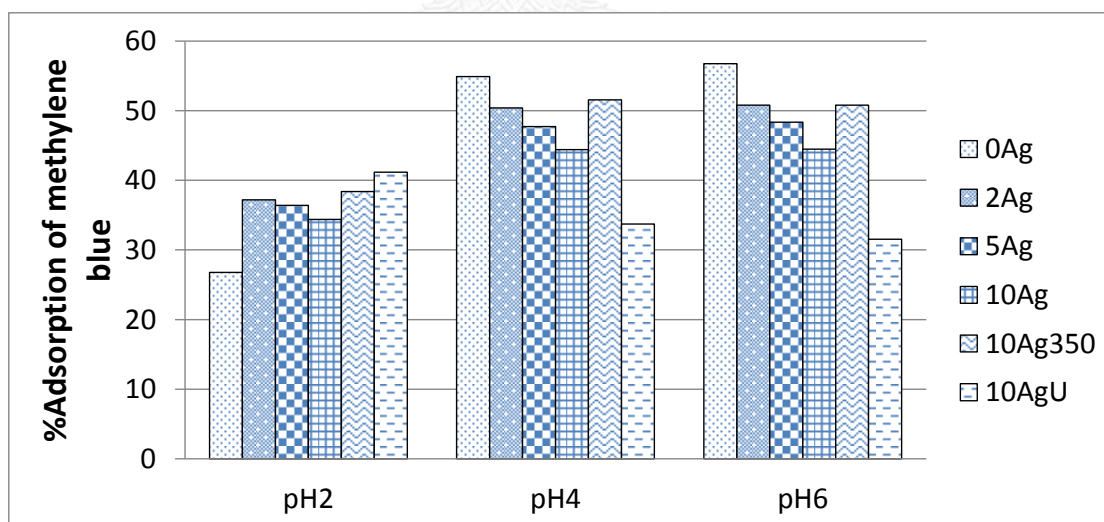
Figure 4.15 Effect of adsorption in acidic condition for the adsorption of methylene blue.

pH of the solution plays an important role in the adsorption process. Solution pH affects both aqueous chemistry and surface binding sites of the

adsorbents. In present investigations, the effect of solution pH on the adsorption of methylene blue was studied over a pH range of 2–6. The experimental results obtained from the investigations are displayed in Figure 4.15. For the pH value of 2, the lowest removal of methylene blue is 26.7% for the host material instead of the highest percent removal of methylene blue. Because the change in solution pH affects the surface charge of alumina by protonation surface functional groups of Al-OH, therefore, it increases in interionic repulsion between cationic dye species and the surface of alumina. The other fibers except uncalcined 10%w/w Ag/Al_2O_3 fibers show that similar trend to the results of maximum capacity for the adsorption of methylene blue as previous described. Thus, it can be confirmed that adding the silver on the alumina fiber increased the adsorption capacity of methylene blue. Our results were agreed with others where silver loaded on alumina adsorbents were effective in the removal of sulphur organic compound such as thiophene [43, 44]. However, the percent removal of methylene blue of uncalcined 10%w/w Ag/Al_2O_3 fibers is decreased from 41.1 to 31.5% with increasing the pH value of 4 to 6. This behavior could be explained by the competition of Ag^+ ions with cationic dye ions for the adsorption on alumina surface. At the lowest pH, $AgNO_3$ which precipitated on fibers is dissociated and precipitated with Cl^- ions, which is used as acid agent, to form AgCl that result in decreasing Ag^+ from the solution and thus resulted in availability of dye ions sorption.

4.2.3 Photocatalytic degradation of methylene blue by Ag/Al$_2$O$_3$ fibers

Figure 4.16 and 4.17 show the removal efficiency of methylene blue by photocatalytic degradation process, which illuminated under LED lamp and sun light, respectively. As a result, under prolonged LED light irradiation, the fibers remove about 20% of methylene blue from its aqueous solution in 100 minutes. However, under sun light irradiation, the fibers remove about 80% of methylene blue from its aqueous solution at equal exposure time. It is speculated that the efficiency of photocatalytic degradation under sun light irradiation was higher about 60% than that under LED light irradiation. This might caused by the higher intensity of photon in sun light than LED light.
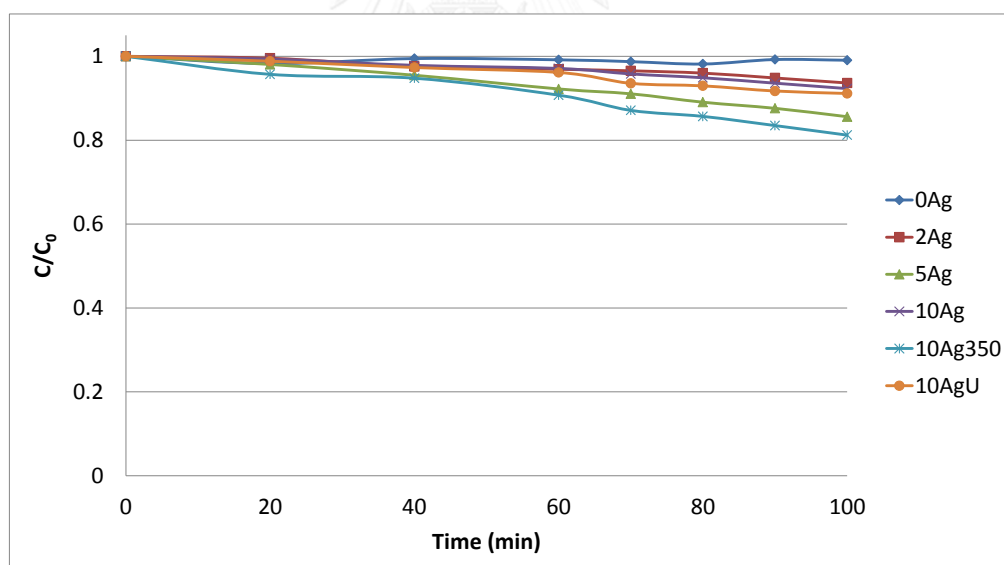
Figure 4.16 Kinetics of methylene blue photodegradation illuminated under LED light.
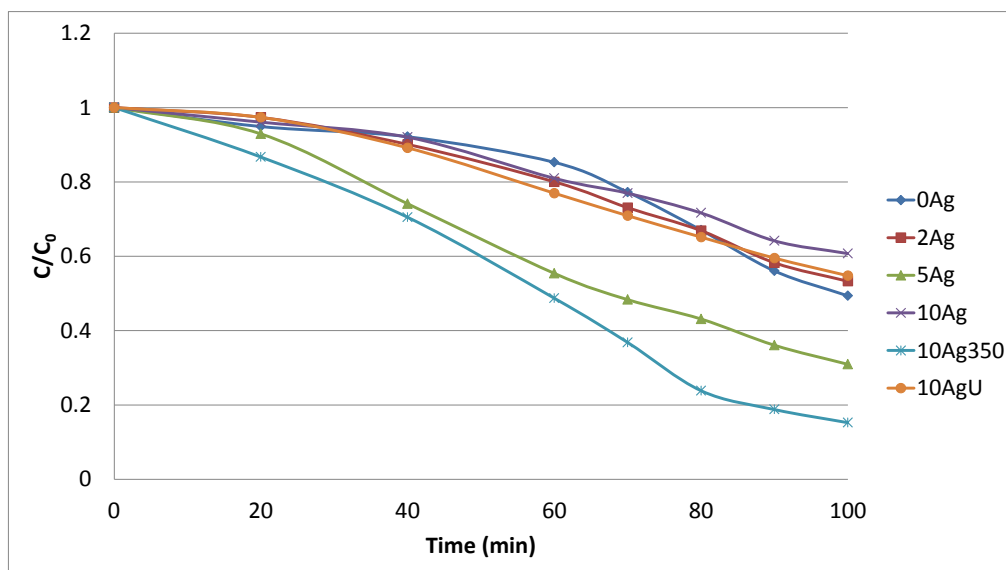
Figure 4.17 Kinetics of methylene blue photodegradation illuminated under sun light.

In this study, we used a first order kinetic model as the simplification of the Langmuir–Hinshelwood (L–H) kinetic model, due to a dilute concentration of methylene blue in the reaction solution [45]. Moreover, the (L–H) model is the most commonly used kinetic expression to explain the kinetics of heterogeneous catalytic reactions. In this model, the reaction rate r can be expressed as below.

$$r = ln\left(\frac{C}{C_0}\right) = -Kt$$

Where C is the concentration of methylene blue at time t, C_0 is the equilibrium concentration after adsorption and K is the apparent rate constant. From the plot of $ln(C/C_0)$ versus irradiation time, a good linear correlation of the data points could be obtained. The linear regressions associated to the pseudo first order rate constant (K).

Table 4.5 Photocatalytic degradation of methylene blue.

Fibers	LED Light		Sun light	
	K (min^{-1})	R^2	K (min^{-1})	R^2
0Ag	-	-	0.0083	0.8674
2Ag	0.0007	0.9500	0.0077	0.9587
5Ag	0.0017	0.9932	0.0138	0.9966
10Ag	0.0009	0.9581	0.0060	0.9632
10Ag350	0.0022	0.9614	0.0231	0.9622
10AgU	0.0011	0.9667	0.0074	0.9875

The estimated first order reaction rate constants for the first order kinetic are presented in Table 4.5. The Al_2O_3 fibers did not show photocatalytic degradation behaviors under LED light irradiation. However, the Al_2O_3 fibers are found to be photoexcited under sun light irradiation with K value of 0.0078 min^{-1}. Even though the band gap of alumina was at about 7.0-7.6 eV, The observed reaction over alumina is due to the surface Lewis acid sites of alumina which promotes the formation of dye cation radicals and thus facilitates dye degradation up on light. For the Ag/Al_2O_3 fibers, the apparent rate constant for methylene blue photodegradation were 0.0007, 0.0017, 0.0009, 0.0022 and 0.0011 min^{-1} (under LED light) and 0.0077, 0.0138, 0.0060, 0.0231 and 0.0074 min^{-1} (under sun light) for calcined 2, 5 and 10 %w/w Ag/ Al_2O_3 fibers at 500 $^{\circ}$C, calcined 10 %w/w Ag/Al_2O_3 fibers at 350 $^{\circ}$C and uncalcined 10 %w/w Ag/Al_2O_3 fibers, respectively. It might be argued that the enhancement in photocatalytic activity among the calcined 2, 5 and 10 %w/w Ag/Al_2O_3 fibers at 500 $^{\circ}$C is not due to the presence of a higher concentration of Ag particles but the larger surface area of particles with a smaller Ag size particles. By

comparing the uncalcined 10 %w/w Ag/Al_2O_3 fibers, calcined 10 %w/w Ag/Al_2O_3 fibers at 350 and 500 $^\circ$C, the highest performance was observed with calcined 10 %w/w Ag/Al_2O_3 fibers at 350 $^\circ$C due to the existence of Ag_2O particles. The narrow band gap of Ag_2O, less than 1.3 eV, resulted in the higher photocatalytic performance of Ag/Al_2O_3 fibers. However, the uncalcined 10 %w/w Ag/Al_2O_3 fibers show slightly better performance than calcined 10 %w/w Ag/Al_2O_3 fibers at 500 $^\circ$C due to smaller Ag particles sizes.

For practical use, the total removal of methylene blue was result from the adsorption process and photocatalytic degradation and summarized in Table 4.6. Only calcined 5 %w/w Ag/Al_2O_3 fibers at 500 $^\circ$C and calcined 10 %w/w Ag/Al_2O_3 fibers at 350 $^\circ$C show higher performance for removal of methylene blue by 7.0% and 15.5% than the host material alumina, respectively.

Table 4.6 Percent removal of methylene blue by adsorption and photocatalytic degradation.

Fibers	%Removal of methylene blue					
	LED light			Sun light		
	Adsorption	Photo-catalytic degradation	Total removal	Adsorption	Photo-catalytic degradation	Total removal
0Ag	54.8	0	54.8	54.8	25.0	79.8
2Ag	50.4	3.0	53.4	50.4	25.3	75.7
5Ag	45.7	6.0	51.7	45.7	41.1	86.8
10Ag	38.1	5.7	43.8	38.1	25.5	63.6
10Ag350	47.3	9.1	56.4	47.3	48.0	95.3
10AgU	26.0	8.3	34.3	26.0	34.4	60.4

4.2.4 Reusability
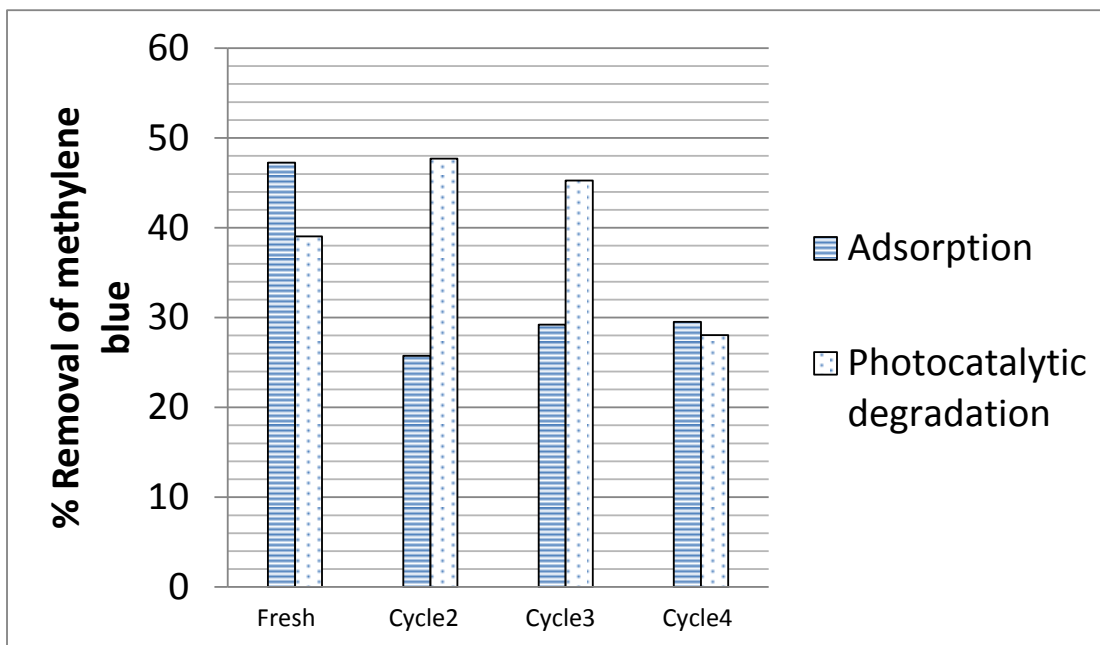
Figure 4.18 Reusability tests of the 5%w/w Ag/Al$_2$O$_3$ fibers.

To verify the reusability of Ag/Al$_2$O$_3$ fibers, repeated removal of MB tests were performed over the calcined 5 %w/w Ag/Al$_2$O$_3$ fibers at 500 $^\circ$C. After each of the photocatalytic cycles, the fibers were separated from the solution, washed with water and dried at 80 $^\circ$C. Over four adsorption cycles, the adsorption efficiency, as shown in Figure 4.18, was lost after the first cycle about 18 %. However, the photocatalytic performance of the fibers was not changed about 45.0 – 47.7 % up to cycle 3 of the removal of methylene blue.

CHAPTER V

CONCLUSION

5.1 Conclusion

The electrospun Ag/Al_2O_3 fibers with various silver concentration (2,5 and 10%w/w) and calcination at 350 and 500 $^{\circ}$C were prepared by the sol–gel electrospinning and conventional impregnation methods using aluminium isopropoxide (AIP) as an alumina precursor, PVA as an a template agent and $AgNO_3$ as a silver precursor. The produced fibers were characterized by SEM, TEM, FT-IR, UV-VIS, XRD and nitrogen adsorption/desorption. From the SEM images of alumina fibers, the average diameters of the fabricated alumina fibers in this study were 75 nm. The silver particles with average diameter of 3-13 nm were observed by TEM. The average particle diameter of the silver particles were increased with increasing silver concentration and calcination temperature. On the basis of the results of the FT-IR, UV-VIS and XRD, the alumina fibers were identified as comprising the γ-alumina phase. The uncalcined Ag/Al_2O_3 fibers have had $AgNO_3$ particles which are precipitated on the surface of alumina after impregnation process and decomposed to form Ag and Ag_2O particles. The results of nitrogen adsorption/desorption were shown that the fibers were a characteristics of mesoporous material and surface area ranged from 171-240 m^2/g. Then, the electrospun Ag/Al_2O_3 fibers were evaluated as a sorbent and a catalyst for removal of methylene blue. As a result, the capacity for adsorption of methylene blue was decreased when silver was incorporated at neutral condition. However, in the acidic condition (pH=2), the capacity for adsorption of methylene blue was increased. In addition, Ag_2O particles enhances the removal of methylene blue both adsorption and photocatalytic reaction. Thus, the demonstrated removal efficiency of methylene blue of Ag loaded alumina fibers further the possibility of utilizing synthetic alumina which is a nontoxic, eco-friendly ceramic for environmental applications and reusable.

5.2 Recommendation for future work

From the preparation of electrospun Ag/Al_2O_3 from as-spun AIP/PVA composite nanofibers, by solgel-electrospinning techniques, and the efficiency for the removal of methylene blue dye in this work, Some recommendations for future studied are proposed as follows:

1. Other metal oxide support such as SiO_2 and TiO_2 should be further investigated.

2. Other metal nanoparticles such as Ni and Cu are interested to study in the photocatalytic reaction.

3. Incipient wetness impregnation should be further studied.

REFERENCES

[1]   Suzuki, F., Onozato, K., and Kurokawa, Y. A formation of compatible poly(vinyl alcohol)/alumina gel composite and its properties. Journal of Applied Polymer Science 39(2) (1990): 371-381.

[2]   Kim, J.-H., et al. Characterization and application of electrospun alumina nanofibers. Nanoscale Research Letters 9(1) (2014): 44-44.

[3]   Stevenson, A.P.Z., Blanco Bea, D., Civit, S., Antoranz Contera, S., Iglesias Cerveto, A., and Trigueros, S. Three strategies to stabilise nearly monodispersed silver nanoparticles in aqueous solution. Nanoscale Research Letters 7(1) (2012): 151-151.

[4]   Polte, J. Fundamental growth principles of colloidal metal nanoparticles - a new perspective. CrystEngComm 17(36) (2015): 6809-6830.

[5]   Balachandran, Y.L., Girija, S., Selvakumar, R., Tongpim, S., Gutleb, A.C., and Suriyanarayanan, S. Differently Environment Stable Bio-Silver Nanoparticles: Study on Their Optical Enhancing and Antibacterial Properties. PLOS ONE 8(10) (2013): e77043.

[6]   Saranya.V.T.K and Gowrie, S.U. Photo Catalytic Reduction of Methylene Blue Dye Using Biogenic Silver Nanoparticles From The Aqueous Cladode Extract of Casuarina Equisetifolia. Indo American Journal of Pharmaceutical Research 6 (2016).

[7]   Chen, K.-H., et al. Ag-Nanoparticle-Decorated SiO_2 Nanospheres Exhibiting Remarkable Plasmon-Mediated Photocatalytic Properties. The Journal of Physical Chemistry C 116(35) (2012): 19039-19045.

[8]   Jiang, W., et al. Silver Oxide as Superb and Stable Photocatalyst under Visible and Near-Infrared Light Irradiation and Its Photocatalytic Mechanism. Industrial & Engineering Chemistry Research 54(3) (2015): 832-841.

[9]   AZAD, A.-M., NOIBI, M., and RAMACHANDRAN, M. Fabrication and characterization of 1-D alumina (Al2O3) nanofibers in an electric field.

BULLETIN OF THE POLISH ACADEMY OF SCIENCES TECHNICAL SCIENCES 55(2) (2007): 195-201.

[10]   Kaur, N., Khanna, A., Chen, B., and González, F. Structural transitions in alumina nanoparticles by heat treatment. AIP Conference Proceedings 1731(1) (2016): 030027.

[11]   Lamouri, S., et al. Control of the γ-alumina to α-alumina phase transformation for an optimized alumina densification. Boletín de la Sociedad Española de Cerámica y Vidrio 56(2) (2017): 47-54.

[12]   Lee, W.E. Ceramic Microstructures: Property control by processing. London, UK: Chapman & Hall, 1994.

[13]   Santos, P.S., Santos, H.S., and Toledo, S.P. Standard transition aluminas. Electron microscopy studies. Materials Research 3 (2000): 104-114.

[14]   Ulusal, F., Darendeli, B., Erünal, E., Egitmen, A., and Guzel, B. Supercritical carbondioxide deposition of γ-Alumina supported Pd nanocatalysts with new precursors and using on Suzuki-Miyaura coupling reactions. The Journal of Supercritical Fluids 127 (2017): 111-120.

[15]   Zhang, L., Wang, X., Chen, C., Zou, X., Ding, W., and Lu, X. Dry reforming of methane to syngas over lanthanum-modified mesoporous nickel aluminate/γ-alumina nanocomposites by one-pot synthesis. International Journal of Hydrogen Energy 42(16) (2017): 11333-11345.

[16]   Esmaeilirad, M., Zabihi, M., Shayegan, J., and Khorasheh, F. Oxidation of toluene in humid air by metal oxides supported on γ-alumina. Journal of Hazardous Materials 333 (2017): 293-307.

[17]   Vosoughi, V., Badoga, S., Dalai, A.K., and Abatzoglou, N. Modification of mesoporous alumina as a support for cobalt-based catalyst in Fischer-Tropsch synthesis. Fuel Processing Technology 162 (2017): 55-65.

[18]   Khabibullin, A., et al. Grafting PMMA Brushes from α-Alumina Nanoparticles via SI-ATRP. ACS Applied Materials & Interfaces 8(8) (2016): 5458-5465.

[19]   Saha, S. Preparation of alumina by sol-gel process, its structures and properties. Journal of Sol-Gel Science and Technology 3(2) (1994): 117-126.

[20]   Ishiguro, K., Ishikawa, T., Kakuta, N., Ueno, A., Mitarai, Y., and Kamo, T. Characterization of alumina prepared by sol-gel methods and its application to MoO3/CoO/Al2O3 catalyst. Journal of Catalysis 123(2) (1990): 523-533.

[21]   Tsubokawa, N., Ogasawara, T., Inaba, J., and Fujiki, K. Carbon black/alumina gel composite: Preparation by sol-gel process in the presence of polymer-grafted carbon black and its electric properties. Journal of Polymer Science Part A: Polymer Chemistry 37(18) (1999): 3591-3597.

[22]   Aqueous and Nonaqueous Sol-Gel Chemistry. in Metal Oxide Nanoparticles in Organic Solvents: Synthesis, Formation, Assembly and Application, pp. 7-18. London: Springer London, 2009.

[23]   Ramakrishna, S., Fujihara, K., Teo, W.-E., Yong, T., Ma, Z., and Ramaseshan, R. Electrospun nanofibers: solving global issues. Materials Today 9(3) (2006): 40-50.

[24]   Ogunlaja, A.S., Kleyi, P.E., Walmsley, R.S., and Tshentu, Z.R. Nanofiber-supported metal-based catalysts. in Catalysis: Volume 28, pp. 144-174: The Royal Society of Chemistry, 2016.

[25]   Biographies. in Nanofiber Composites for Biomedical Applications, pp. xv-xvi: Woodhead Publishing, 2017.

[26]   Zhu, N. and Chen, X. Biofabrication of Tissue Scaffolds Advances in Biomaterials Science and Biomedical Applications. Advances in Biomaterials Science and Biomedical Applications 2013.

[27]   Kim, M.-R., Park, S.-H., Kim, J.-U., and Lee, J.-K. Dye-Sensitized Solar Cells Based on Polymer Electrolytes. 2011.

[28]   Gürses, A., Açıkyıldız, M., Güneş, K., and Gürses, M.S. Dyes and Pigments: Their Structure and Properties. in Dyes and Pigments, pp. 13-29. Cham: Springer International Publishing, 2016.

[29]   Pirkarami, A. and Olya, M.E. Removal of dye from industrial wastewater with an emphasis on improving economic efficiency and degradation mechanism. Journal of Saudi Chemical Society 21, Supplement 1 (2017): S179-S186.

[30] Bharathi, K.S. and Ramesh, S.T. Removal of dyes using agricultural waste as low-cost adsorbents: a review. Applied Water Science 3(4) (2013): 773-790.

[31] Distinguish between Physical Adsorption and Chemisorption.

[32] Chemisorption and physisorption [Online]. Available from: http://old.iupac.org/reports/2001/colloid_2001/manual_of_s_and_t/node16.html

[33] Banerjee, S., Gautam, R.K., Jaiswal, A., Chandra Chattopadhyaya, M., and Chandra Sharma, Y. Rapid scavenging of methylene blue dye from a liquid phase by adsorption on alumina nanoparticles. RSC Advances 5(19) (2015): 14425-14440.

[34] Allen, S.J., McKay, G., and Porter, J.F. Adsorption isotherm models for basic dye adsorption by peat in single and binary component systems. Journal of Colloid and Interface Science 280(2) (2004): 322-333.

[35] Chin, S., Park, E., Kim, M., and Jurng, J. Photocatalytic degradation of methylene blue with TiO2 nanoparticles prepared by a thermal decomposition process. Powder Technology 201(2) (2010): 171-176.

[36] Chen, X., Wu, Z., Liu, D., and Gao, Z. Preparation of ZnO Photocatalyst for the Efficient and Rapid Photocatalytic Degradation of Azo Dyes. Nanoscale Research Letters 12 (2017): 143.

[37] Sarina, S., Waclawik, E.R., and Zhu, H. Photocatalysis on supported gold and silver nanoparticles under ultraviolet and visible light irradiation. Green Chemistry 15(7) (2013): 1814-1833.

[38] Guo, X., Hao, C., Jin, G., Zhu, H.-Y., and Guo, X.-Y. Copper Nanoparticles on Graphene Support: An Efficient Photocatalyst for Coupling of Nitroaromatics in Visible Light. Angewandte Chemie International Edition 53(7) (2014): 1973-1977.

[39] Photocatalyst Mosquito Trap_Principle [Online]. Available from: http://www.supesolar.com/mosquito-fly-trap/photocatalyst-mosquito-trap-principle.htm

[40]   Gangwar, J., Gupta, B.K., Tripathi, S.K., and Srivastava, A.K. Phase dependent thermal and spectroscopic responses of Al_2O_3 nanostructures with different morphogenesis. Nanoscale 7(32) (2015): 13313-13344.

[41]   Zhang, L., Zhang, C., and He, H. The role of silver species on Ag/Al_2O_3 catalysts for the selective catalytic oxidation of ammonia to nitrogen. Journal of Catalysis 261(1) (2009): 101-109.

[42]   Kuila, U. and Prasad, M. Specific surface area and pore-size distribution in clays and shales. Geophysical Prospecting 61(2) (2013): 341-362.

[43]   Liao, J., Wang, Y., Chang, L., and Bao, W. Preparation of M/[gamma]-Al_2O_3 sorbents and their desulfurization performance in hydrocarbons. RSC Advances 5(77) (2015): 62763-62771.

[44]   Jeevanandam, P., Klabunde, K.J., and Tetzler, S.H. Adsorption of thiophenes out of hydrocarbons using metal impregnated nanocrystalline aluminum oxide. Microporous and Mesoporous Materials 79(1) (2005): 101-110.

[45]   Mondal, S., De Anda Reyes, M.E., and Pal, U. Plasmon induced enhanced photocatalytic activity of gold loaded hydroxyapatite nanoparticles for methylene blue degradation under visible light. RSC Advances 7(14) (2017): 8633-8645.

APPENDIX
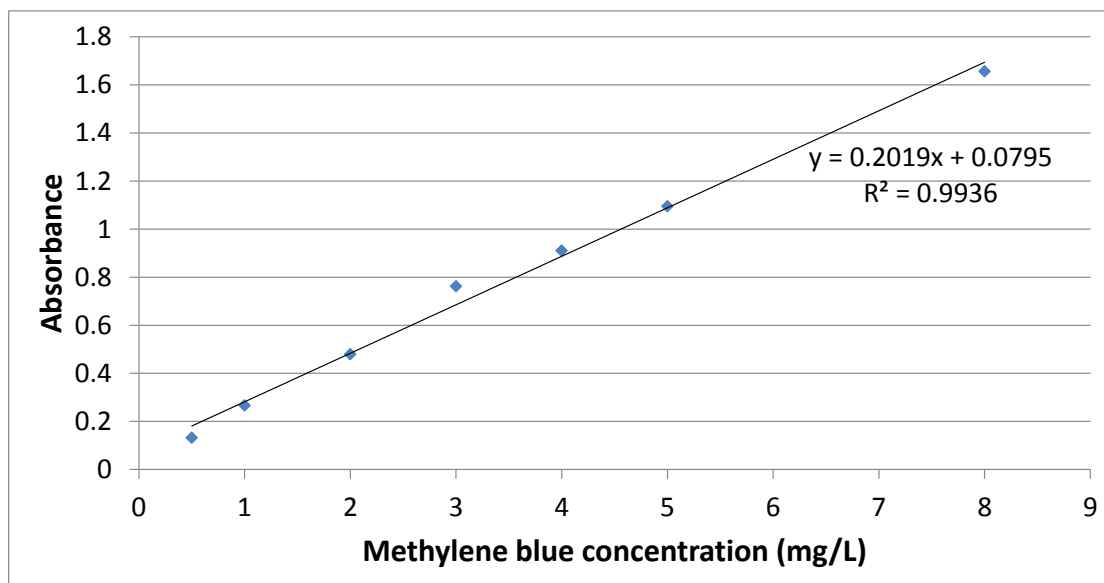
Calibration curve of methylene blue

Figure A.1 Calibration curve for methylene blue solution.

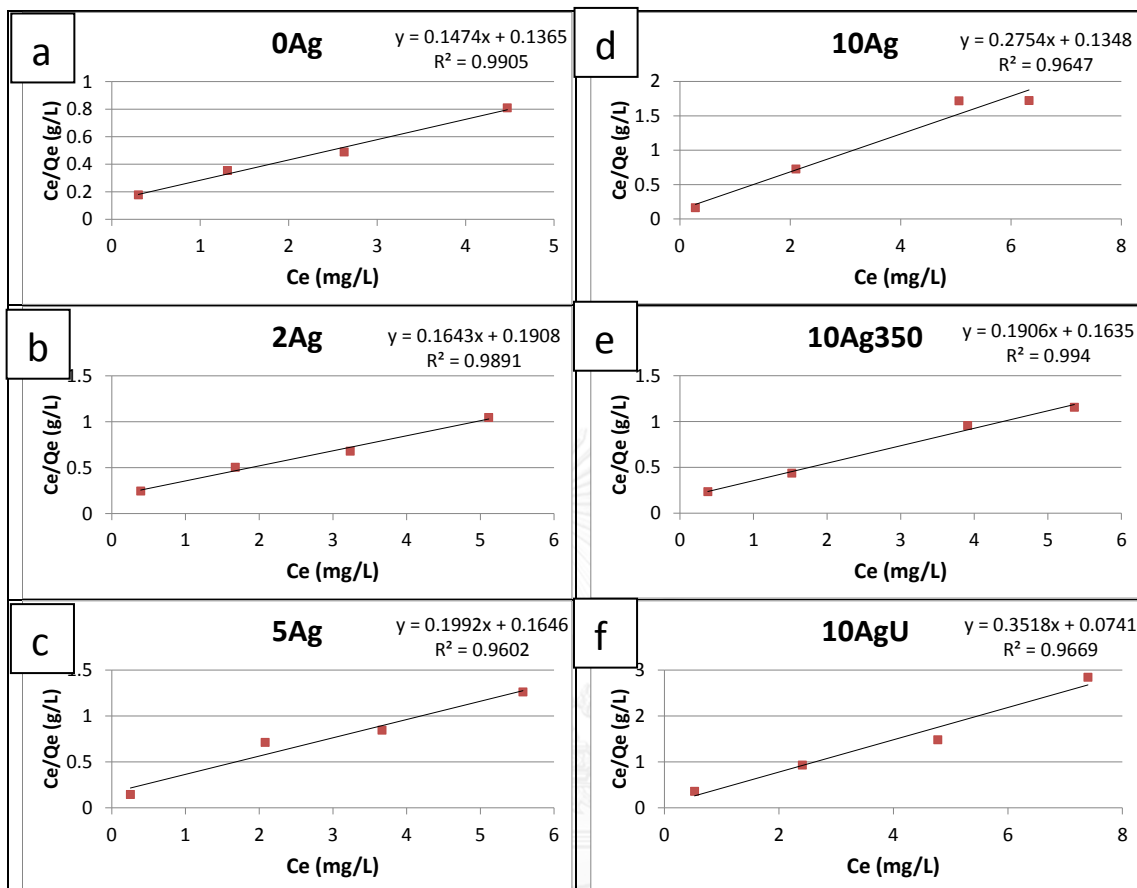## Langmuir plot for the adsorption of methylene blue

Figure A.2 Langmuir plot for the adsorption of methylene blue of (a) Al_2O_3 fibers (b) 2%w/w Ag/Al_2O_3 fibers (500 $^\circ$C calcination) (c) 5%w/w Ag/Al_2O_3 fibers (500 $^\circ$C calcination) (d) 10%w/w Ag/Al_2O_3 fibers (500 $^\circ$C calcination) (e) 10%w/w Ag/Al_2O_3 fibers (350 $^\circ$C calcination) (f) 10%w/w Ag/Al_2O_3 fibers (uncalcination).
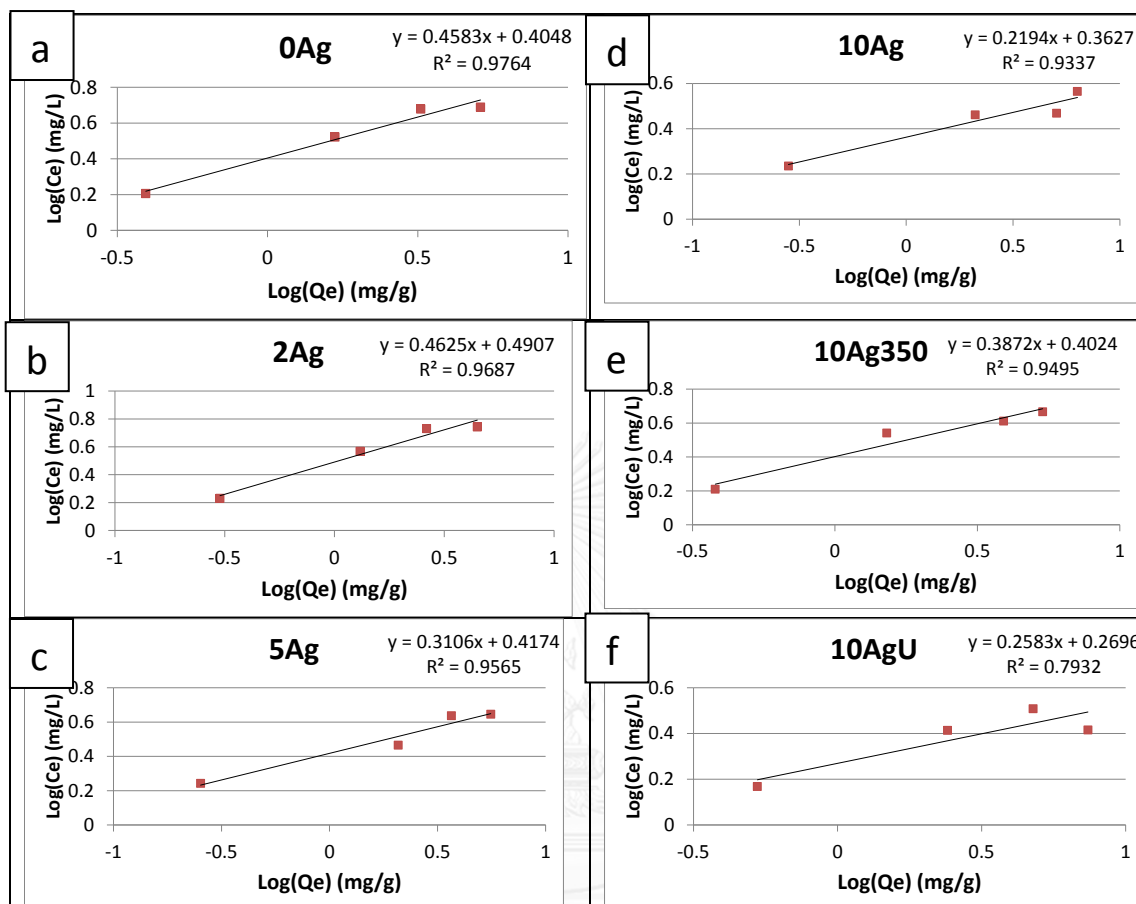
Freundlich plot for the adsorption of methylene blue

Figure A.3 Freundlich plot for the adsorption of methylene blue of (a) Al_2O_3 fibers (b) 2%w/w Ag/Al_2O_3 fibers (500 $^\circ$C calcination) (c) 5%w/w Ag/Al_2O_3 fibers (500 $^\circ$C calcination) (d) 10%w/w Ag/Al_2O_3 fibers (500 $^\circ$C calcination) (e) 10%w/w Ag/Al_2O_3 fibers (350 $^\circ$C calcination) (f) 10%w/w Ag/Al_2O_3 fibers (uncalcination).

The Langmuir-Hinshelwood model

The rate equation is used in the form

$$\frac{-dC}{dt} = \frac{k_{L\text{-}H} K_{ad} C}{1 + K_{ad} C}$$

Where K_{ad} is the adsorption coefficient of the reactant on fibers, $k_{L\text{-}H}$ is the reaction rate constant and C is the concentration at any time t. The values of $k_{L\text{-}H}$ and K_{ad} are used to explain the effect of light intensity on the equilibrium constant. Then, by integration of above equation.

$$\text{Ln}\left(\frac{C_0}{C}\right) = K(C - C_0) + k_{L\text{-}H} K_{ad} t$$

where C_0 is the initial concentration. For pseudo-first-order reaction K_{ad}. C is very small compared to 1, so it is simplified and integrated to be:

$$\text{Ln}\left(\frac{C_0}{C}\right) = k_{L\text{-}H} K_{ad} t = kt$$

where $k = k_{L\text{-}H} K_{ad}$ is the pseudo-first-order reaction rate constant

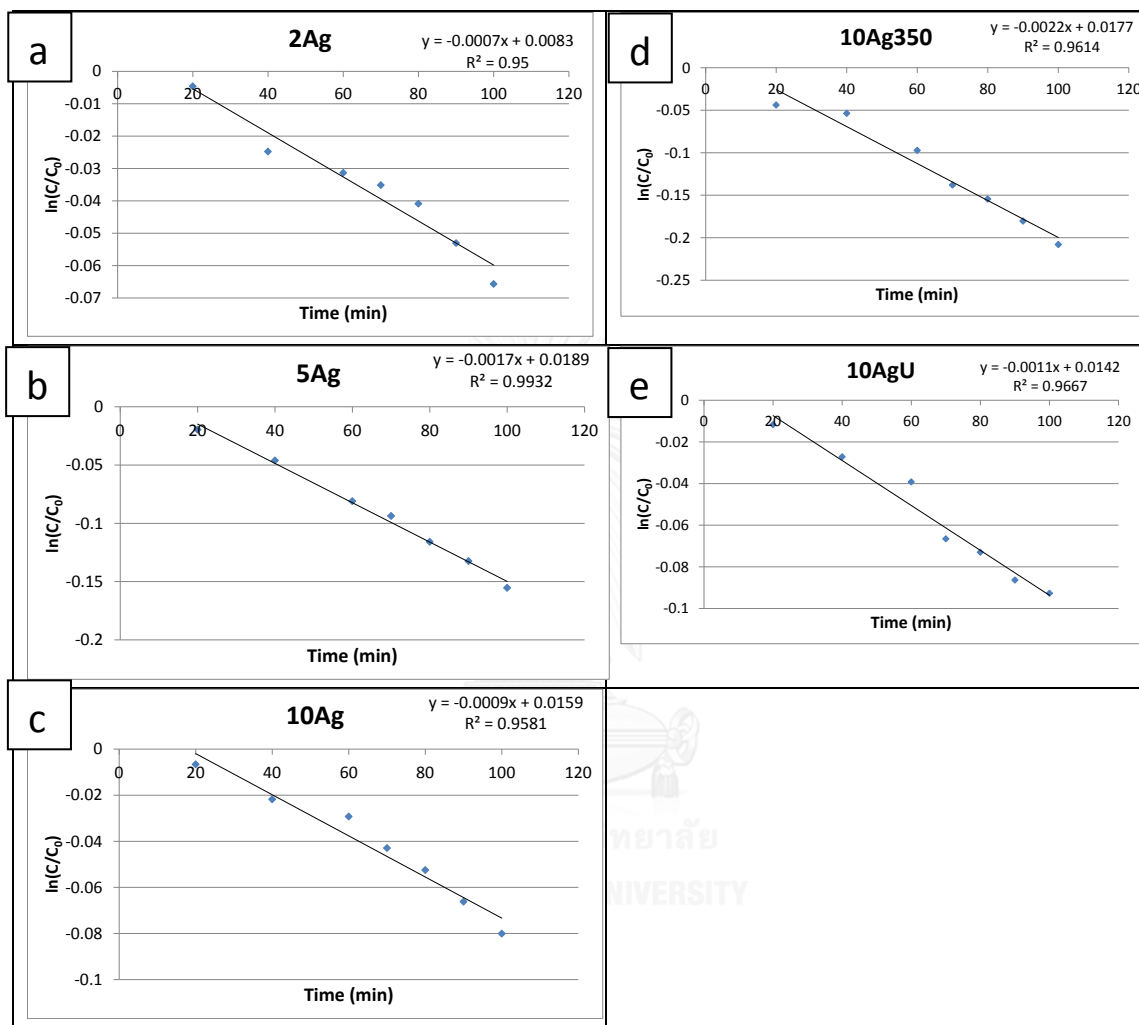L–H kinetic model first order plots for kinetic photodegradation of methylene blue illuminated under LED light

Figure A.4 L–H kinetic model first order plots for kinetic photodegradation of methylene blue illuminated under LED light of (a) 2%w/w Ag/Al_2O_3 fibers (500 $^{\circ}$C calcination) (b) 5%w/w Ag/Al_2O_3 fibers (500 $^{\circ}$C calcination) (c) 10%w/w Ag/Al_2O_3 fibers (500 $^{\circ}$C calcination) (d) 10%w/w Ag/Al_2O_3 fibers (350 $^{\circ}$C calcination) (e) 10%w/w Ag/Al_2O_3 fibers (uncalcination).

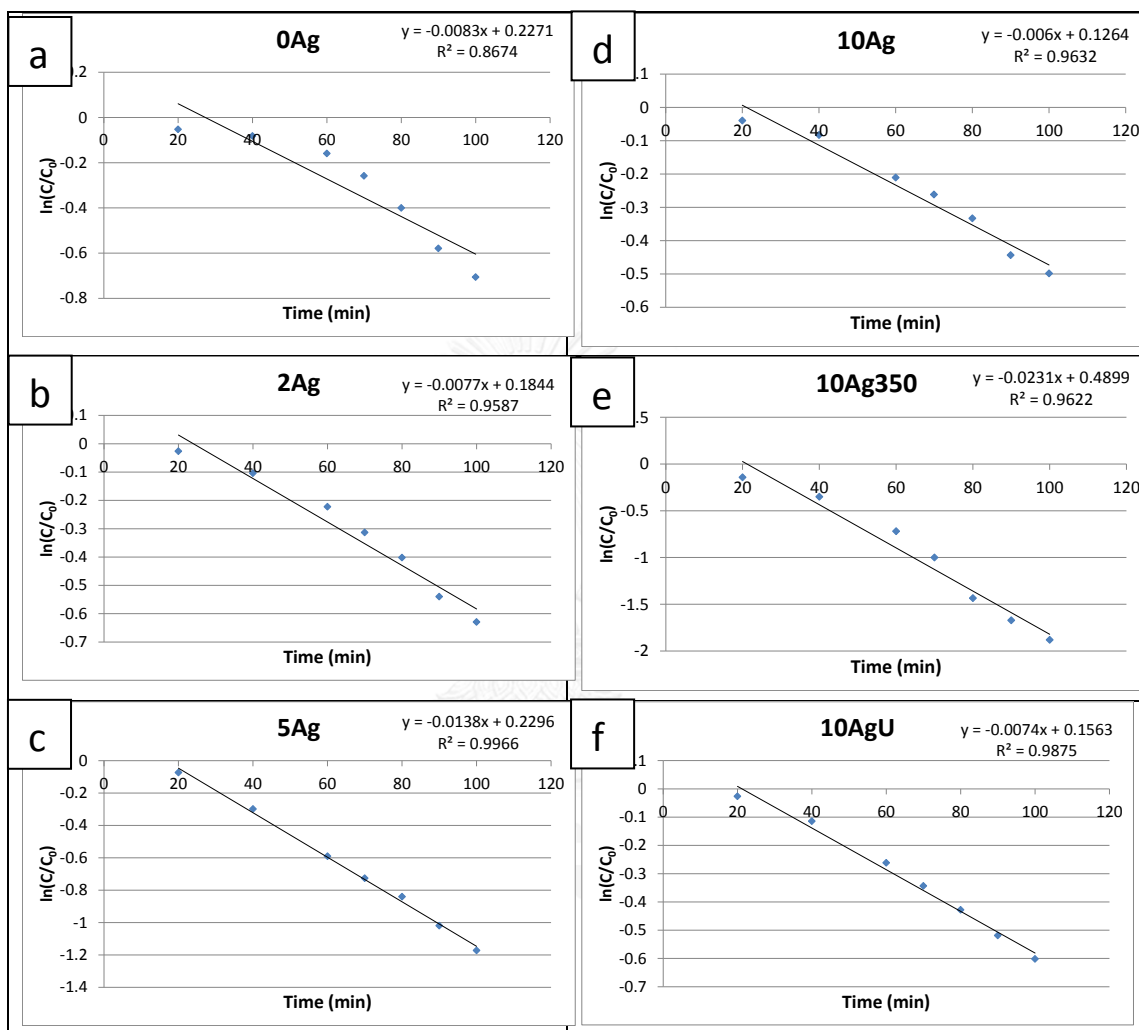L–H kinetic model first order plots for kinetic photodegradation of methylene blue illuminated under sun light

Figure A.5 L–H kinetic model first order plots for kinetic photodegradation of methylene blue illuminated under sun light of (a) 2%w/w Ag/Al$_2$O$_3$ fibers (500 $^\circ$C calcination) (b) 5%w/w Ag/Al$_2$O$_3$ fibers (500 $^\circ$C calcination) (c) 10%w/w Ag/Al$_2$O$_3$ fibers (500 $^\circ$C calcination) (d) 10%w/w Ag/Al$_2$O$_3$ fibers (350 $^\circ$C calcination) (e) 10%w/w Ag/Al$_2$O$_3$ fibers (uncalcination).

VITA

Mr.Parom Waikasikarn was born on 3 Aug 1992 in Bangkok, Thailand. He graduated with degree of Bachelor of Science in Chemistry, King Mongkut's University of Technology Thonburi in 2014. After that, he has been a graduated student at Program of Petrochemistry and Polymer Science, Chulalongkorn University and become a member of Chromatography and Separation Research Unit (ChSRU). He finished his Master's degree of Science in 2017.

Poster presentation and proceeding

"Characterization of electrospun Ag/Al2O3 fibers for selective catalytic oxidation" Pure and Applied Chemistry International Conference 2017 (PACCON 2017).